High-Order Perturbation of Surfaces Approach to Fokas Integral Equations: Maxwell Equations

by

Venu Madhav Tammali
B.E. (Vasavi College, Osmania University)
M.S. (Courant Institute, New York University)

Thesis submitted in partial fulfillment of the requirements
for the degree of Doctor of Philosophy in Mathematics
in the Graduate College of the
University of Illinois at Chicago, 2015

Chicago, Illinois

Defense Committee:
David P. Nicholls, Chair and Advisor
Shmuel Friedland
Alexey Cheskidov
Christof Sparber
Gerard Awanou
Misun Min, Argonne National Lab

To my parents and sister, who have let me do whatever I want to do.

ACKNOWLEDGMENTS

I want to thank my advisor Prof. David Nicholls for his generous time and steadfast support. Without his strong support, I wouldn't have been able to join UIC after I deferred my admission. He gave me enough time to explore my interests. He always found time for me and helped me make right choices to finish my PhD. He provided me a great opportunity to intern at Argonne National Lab. He not only taught me mathematics but also many a valuable life principles. He was very flexible and understanding. My stay at UIC has been almost stress free because I knew I had my advisor who would help me out if I face deadends. He was also very encouraging to work with other Professors. I couldn't have wished for a better advisor. I would miss my weekly interactions with him dearly after I leave UIC. I hope to continue to be in touch with him in the future.

I would also like to thank Prof. Shmuel Friedland. I consider myself lucky to have met him. His calm and joyous demeanor will have an everlasting impression on me. I was fortunate enough to cowrite a paper with him. I am ever so grateful to many of his kind gestures. Many of his wise words had a profound impression on me.

Lastly, I would like to acknowledge Tasos Moulinos and Sam Ziegler for making my stay at UIC filled with so many great memories. Whenever I felt tired and down, they helped me get back with their humor. They both taught me how to be good at something and be humble at the same time.

TABLE OF CONTENTS

LIST OF FIGURES

FIGURE **PAGE**

SUMMARY

The accurate simulation of linear electromagnetic scattering by diffraction gratings is crucial in several technologies of scientific interest. In this contribution we describe a High–Order Perturbation of Surfaces (HOPS) algorithm built upon a class of Integral Equations due to the analysis of Fokas and collaborators, now widely known as the Unified Transform Method. The unknowns in this formalism are boundary quantities (the electric field and current at the layer interface) which are an order of magnitude fewer than standard volumetric approaches such as Finite Differences and Finite Elements. Our numerical experiments show the efficiency, fidelity, and high–order accuracy of our algorithm.

CHAPTER 1

INTRODUCTION

We first introduce the setting of Fokas Integral equations and our HOPS approach built on these equations to solve scalar Helmholtz equations satisfied by electro-magnetic waves diffracted across a periodic structure. We later build on the framework established for the Helmholtz equation to solve the vector Maxwell equation satisfied by electromagnetic waves diffracted across a periodic structure.

1.1 Volumetric methods

Classical numerical algorithms such as Finite Elements (e.g., (1; 2; 3; 4)) and Finite Differences (e.g., (5; 6; 7)) have been used to simulate these configurations. Volumetric approaches however have prohibitively large number of unknowns for the piecewise homogeneous grating problem we consider here. In addition, for these methods an error is introduced by enforcing an (approximately) "Non–Reflecting Boundary Condition" (e.g., (8) and variants, e.g., (9; 10; 11)) by restricting the unrestricted problem domain at some finite distance from the grating structure.

1.2 Boundary Integral methods

Consequently, methods based upon Integral Equations (IEs) (12) are a better candidate but they face many limitations. For instance, in order to deliver high–order (spectral) accuracy, special quadrature rules must be designed. These rules result in dense, non–symmetric positive definite linear systems when applied to nonlocal IEs . However, these limitations have been reasonably taken care of (by iterative solution procedures accelerated by Fast Multipole Methods (13)) and hence Boundary Integral methods are a compelling

choice (14). But, the following three properties make them non–competitive compared with our new method for the *periodic*, *parametrized* problems we consider. First, for *periodic* problems the relevant Green function must be periodized. This periodization induces slow convergence, a well–known problem (15). This slow convergence induced can be accelerated (e.g., with Ewald summation). However, these methods necessitate an *additional* discretization parameter: The number of approximate terms retained in periodized Green function.

Second, for crossed interface, parameterized by height/slope ε, an IE solver must be invoked for every ε. Finally, for each simulation the dense, non–symmetric positive definite matrices must be inverted .

1.3 New alternative

Our new method is a "High–Order Perturbation of Surfaces" (HOPS) method, more specifically a Fokas Integral Equation (FIE) formulation appropriately generalized to the fully three–dimensional vector Maxwell equations (16; 17). These formulations have their beginnings to the low–order calculations of Rayleigh (18) and Rice (19). Their high–order version has been developed into the Method of Field Expansions (FE) by Bruno & Reitich (20; 21; 22), Nicholls and Reitich (23; 24; 25), and Nicholls and Malcolm (26; 27). A closely related algorithm, the Method of Operator Expansions, was developed in parallel by Milder and collaborators (28; 29; 30; 31; 32; 33; 34).

These formulations not only have the advantages of classical Integral Equations formulations (e.g., exact enforcement of far–field conditions and surface formulation) but also avoid the shortcomings listed above. First, quasiperiodicity of solutions is manifested itself and does not need to be further approximated as HOPS schemes utilize eigenfunctions of the Laplacian (suitable complex exponentials) on a *periodic* domain.

Second, Once the Taylor coefficients are calculated for the scattering fields, a simple summation for any given boundary parameter ε will recover the returnsIinstead of starting a new simulation) as these methods are built upon expansion in ε.

Finally, we need to only invert a single, sparse operator (flat–interface approximation operator) for every perturbation order .

As shown in (16; 17) for solving the Helmholtz equation the approach of Fokas (35) and collaborators (see, e.g., (36; 37; 38)) allows one to state simple integral relations for Dirichlet and Neumann data of elliptic boundary value problems which do *not* involve the fundamental solution. Instead they feature quite smooth kernels related to solutions of the relevant Helmholtz problem meaning that simple quadrature rules (e.g., Nyström's Method (12)) can be brought to bear on the problem. The Fokas approach (known as the "Unified Transform Method") does lead to dense, poorly conditioned linear systems to be inverted, but it was shown in (17) how this can be significantly ameliorated with a HOPS methodology. In particular, as we shall see, one trades a single dense and ill–conditioned matrix inversion for a sequence (one for each perturbation order retained) of fast, well–conditioned linear solves around the base (flat–interface) geometry. This matrix is of convolution–type which enables rapid solution by the FFT algorithm. Additionally, we find that, for many configurations of interest, a few perturbation orders are sufficient for a solution of high fidelity, resulting in an algorithm of remarkable speed and accuracy.

CHAPTER 2

TWO-DIMENSIONAL SCATTERING: THE HELMHOLTZ EQUATION

We consider the problem of diffraction of electromagnetic waves across a periodic structure. More precisely, we consider two regions, Ω^+ and Ω^-, that are made up of materials with dielectric constants ε^+ and ε^-, respectively or with dielectric constant ε^+ and a perfect conductor respectively. A grating surface $y = f(x)$, where f is a periodic function of period d seperate these regions. We assume the permeability of the dielectrics equal to μ_o, the permeability of vaccum.

When the grating is illuminated by a plane wave

$$\mathbf{E}^i = \mathbf{A}e^{i\alpha x - i\beta y}e^{-i\omega t}, \tag{2.1a}$$

$$\mathbf{H}^i = \mathbf{B}e^{i\alpha x - i\beta y}e^{-i\omega t}, \tag{2.1b}$$

If the two regions are filled with a dielectric and a perfect conductor respectively, the total field in Ω^+ is given by

$$\mathbf{E}^{up} = \mathbf{E}^i + \mathbf{E}^{refl}, \tag{2.2a}$$

$$\mathbf{H}^{up} = \mathbf{H}^i + \mathbf{H}^{refl}, \tag{2.2b}$$

where as the field in Ω^- vanishes. We remove the factor $\exp(-i\omega t)$, and also point that the incident, reflected, and total fields satisfy the time-harmonic Maxwell equations (39)

$$\nabla \times \mathbf{E} = i\omega\mu_o \mathbf{H}, \quad \nabla \cdot \mathbf{E} = 0, \tag{2.3a}$$

$$\nabla \times \mathbf{H} = i\omega\varepsilon^+ \mathbf{E}, \quad \nabla \cdot \mathbf{H} = 0, \tag{2.3b}$$

in Ω^+. And, at the interface between two regions the total field satisfies

$$\mathbf{n} \times \mathbf{E}^{up} = 0 \quad \text{on } y = f(x), \tag{2.4}$$

where $\mathbf{n}$ is the unit vector normal to the interface. If regions Ω^+ and Ω^- are made up of two dielectrics, the total field in Ω^- satifsfies Eqs. (2.3) and holds the following transmission conditions:

$$\mathbf{n} \times (\mathbf{E}^{up} - \mathbf{E}^{down}) = 0, \quad \text{on} \quad y = f(x). \tag{2.5a}$$

$$\mathbf{n} \times (\mathbf{H}^{up} - \mathbf{H}^{down}) = 0, \quad \text{on} \quad y = f(x). \tag{2.5b}$$

$$\tag{2.5c}$$

And finally, the periodic grating surface induces quasi-periodic fields: if v is either $\mathbf{E}$ or $\mathbf{H}$, we have

$$v(x + d, y) = \exp(i\alpha d) v(x, y). \tag{2.6}$$

For the above situation the fields **E** and **H** are independent of z (refer (39)) and Eqs. (2.3) and (2.4) [or Eqs. (2.3) and (2.5)] can be simplified to set of equations for a single unknown. In fact $u(x, y)$ equal to either diffracted E_z(Transverse Electric - TE) or diffracted H_z(Transverse Magnetic - TM) satisfy the Helmholtz equation

$$\Delta u + (k^{\pm})^2 u = 0 \quad \text{in } \Omega^{\pm}, \tag{2.7}$$

where $k^{\pm} = \omega\sqrt{\mu_o \varepsilon^{\pm}}$. Succintly, the solution above is an α-quasi-periodic function which satisifies the Helmholtz equation and one of the following boundary conditions (39).

1. TE Mode: Dielectric-Perfect Conductor Interface

Set $u = E_z^{\text{refl}}$, then the boundary condition is

$$u = -\exp[i\alpha x - i\beta f(x)] \quad \text{on } y = f(x). \tag{2.8}$$

2. TM Mode: Dielectric-Perfect Conductor Interface

Set $u = H_z^{\text{refl}}$, then the boundary condition is

$$\frac{\partial u}{\partial n} = -\frac{\partial}{\partial n}\exp(i\alpha x - i\beta y) \quad \text{on} \quad y = f(x). \tag{2.9}$$

3. TE Mode: Interface between two Dielectrics

Set $u^+ = E_z^{\text{refl}}, u^- = E_z^{\text{refr}}$, then the boundary conditions are

$$u^+ - u^- = -\exp[i\alpha x - i\beta y] \quad y = f(x), \tag{2.10a}$$

$$\frac{\partial u^+}{\partial n} - \frac{\partial u^-}{\partial n} = -\frac{\partial}{\partial n}\exp(i\alpha x - i\beta y) \quad \text{on } y = f(x). \tag{2.10b}$$

4. TM Mode: Interface between Two Dielectrics

Set $u^+ = H_z^{refl}, u^- = H_z^{refr}$, then the boundary conditions are

$$u^+ - u^- = -\exp[i\alpha x - i\beta y] \quad y = f(x), \tag{2.11a}$$

$$\frac{\partial u^+}{\partial n} - (1/\nu_o^2)\frac{\partial u^-}{\partial n} = -\frac{\partial}{\partial n}\exp(i\alpha x - i\beta y) \quad on \;\; y = f(x), \tag{2.11b}$$

where $\nu_o^2 = \frac{\varepsilon^-}{\varepsilon^+} = (\frac{k^-}{k^+})^2$.

2.1 Rayleigh Expansion, Radiation Conditions, and Energy Balance

Lets incorporate boundary conditions at infinity to Eq. (2.7) to determine the soltuion u: The solution should consist of outgoing waves and must be bounded at infinity.

Let

$$K = \frac{2\pi}{d}, \quad \alpha_n = \alpha + nK, \quad \alpha_n^2 + (\beta_n^\pm)^2 = (k^\pm)^2, \tag{2.12}$$

where $\beta_n^\pm$ is determined by $Im\beta_n^\pm > 0$ or $\beta_n^\pm \geq 0$. Assume

$$k^+ \neq \pm(\alpha + nK), \qquad k^- \neq \pm(\alpha + nK) \tag{2.13}$$

where n is any integer. The case $k^\pm = \pm(\alpha + nK)$ for any n are known as Woods anomalies. (Refs. 18 and 19.). This phenomenon is not discussed here, and (2.13) will be assumed to hold.

Under this assumption, in the region Ω^+, for $y > y_M = |f|_\infty$, any α-quasi-periodic solution to the Helmholtz equation is given by the Rayleigh expansion

$$u^+ = \sum_{n=-\infty}^{\infty} A_n^+ \exp(i\alpha_n x - i\beta_n^+ y) + \sum_{n=-\infty}^{\infty} B_n^+ \exp(i\alpha_n x + i\beta_n^+ y). \tag{2.14}$$

Similarly, in Ω^-, for $y < y_m = -|f|_\infty$, any solution u^- to the Helmholtz equation is given by

$$u^- = \sum_{n=-\infty}^{\infty} A_n^- \exp(i\alpha_n x - i\beta_n^- y) + \sum_{n=-\infty}^{\infty} B_n^- \exp(i\alpha_n x + i\beta_n^- y). \tag{2.15}$$

Also solution u of Eq. (2.7) in $\Omega^\pm$ satisfies the radiation condition at infinity if

$$A_n^+ = 0, \quad B_n^- = 0 \quad \text{for all n.} \tag{2.16}$$

Finally, to test the convergence for the numerical solution of diffraction problems, we would use the relation between the Rayleigh coefficients of u given by the principle of conservation of energy (39). For example, if Ω^- is made up with a perfect conductor and if k^+ is real, this energy criterion is given by

$$\sum_{n \in U^+} \beta_n^+ |B_n^+|^2 = \beta_o^+, \tag{2.17}$$

$$\text{Where} \quad U^+ \equiv \{n : \beta_n^+ > 0\}. \tag{2.18}$$

Equivalently

$$\sum_{n \in U^+} e_n = 1, \tag{2.19}$$

where $e_n = \beta_n^+ |B_n^+|^2 / \beta_o^+$. The coefficient e_n is called the nth-order efficiency.

2.2 Theory

When the grating is shaped by $y = f(x) = \varepsilon g(x)$ and g is smooth ($C^2, C^{1+\delta}, \text{Lipschitz}$) the field $u = u(x, y, \varepsilon)$ is analytic with respect to the parameter ε. Under the assumption *f(x)* is analytic, the following results have been established (40).

1. Given a profile $y = \varepsilon_o f(x)$, for some $\varepsilon_o \in \mathbb{R}$ and y_o above (or below) the profile, $u = u(x, y, \varepsilon)$ is an analytic function of $x, y,$ and ε for y sufficiently close to y_o and ε sufficiently close to ε_o.

2. The functions

$$u^{\pm}(x, \varepsilon f(x), \varepsilon), \tag{2.20a}$$

$$\frac{\partial u^{\pm}}{\partial n_{\varepsilon}(x, \varepsilon f(x))}(x, \varepsilon f(x), \varepsilon) \tag{2.20b}$$

are analytic with respect to x and ε.

3. For an $\varepsilon_o \in \mathbb{R}$, the functions $u^{\pm}$ are analytic with respect to ε, x and y for ε close to ε_o and y close to the interface $y = \varepsilon_o f(x)$. This property implies that functions $u^{\pm}$ can be analytically extended across the interface.

It follows from 1 and 3, that $u^{\pm}$ can be expanded in power series of ε,

$$u^{\pm}(x, y, \varepsilon) = \sum_{n=0}^{\infty} u_n^{\pm}(x, y)\varepsilon^n, \tag{2.21}$$

and converge for small ε. The functions $u^{\pm}$ also satisy Helmholtz equations.

From 2 and 3, differentiation of solutions with respect to ε and use of the chain rule are permissible

$$u^+ - u^- = -\exp[i\alpha x - i\beta\varepsilon f(x)] \quad \text{on} \quad y = \varepsilon f(x), \tag{2.22a}$$

$$\frac{\partial u^+}{\partial n_\varepsilon} - \nu_0^2 \frac{\partial u^-}{\partial n_\varepsilon} = -\frac{\partial}{\partial n_\varepsilon}\exp(i\alpha x - i\beta\varepsilon f(x)) \quad \text{on} \quad y = \varepsilon f(x), \tag{2.22b}$$

2.3 Fokas Integral Equations

The Dirichlet-Neumann operator (DNO) in our approach comes from the procedure of Fokas which, in our context, particularly follows from the following identity.

Lemma 2.1. *If we define*

$$Z^{(k)} := \partial_y\phi(\Delta\psi + k^2\psi) + (\Delta\phi + k^2\phi)\partial_y\psi$$

then

$$Z^{(k)} := \mathrm{div}_x[F^{(x)}] + \partial_y[F^{(x)} + F^{(k)}],$$

where

$$F^{(x)} := \partial_y\phi(\nabla_x\psi) + \nabla_x\phi(\partial_y\psi),$$

$$F^{(y)} := \partial_y\phi(\partial_y\psi) - \nabla_x\phi \cdot (\nabla_x\psi),$$

$$F^{(k)} := k^2\phi\,\psi.$$

Defining the periodic domain

$$\Omega = \Omega(\bar{l} + l(x), \bar{u} + u(x)) := \{0 < x < d\} \times \{\bar{l} + l(x) < y < \bar{u} + u(x)\}, \tag{2.23a}$$

$$l(x + d) = l(x), \quad u(x + d) = u(x), \tag{2.23b}$$

provided that ϕ and ψ solve the Helmholtz equations

$$\Delta\phi + k^2\phi = 0, \quad \Delta\psi + k^2\psi = 0, \tag{2.24}$$

then $Z^{(k)} = 0$. A (trivial) consequence of the divergence theorem gives us the following lemma.

Lemma 2.2. *Suppose that* $\boldsymbol{G}(x,y)$*, defined on* Ω*, is d-periodic in the x variable,* $\boldsymbol{G}(x+d,y) = \boldsymbol{G}(x,y)$*, where*

$$\mathbf{G}(x,y) = (G^{(x)}(x,y), G^{(y)}(x,y))^T, \tag{2.25}$$

then

$$\begin{aligned}\int_\Omega div[\mathbf{G}]dV = &\int_0^d [G^{(x)} \cdot (\nabla_x l) - G^{(y)}]_{y=\bar{l}+l(x)}\, dx \\ &+ \int_0^d [-G^{(x)} \cdot (\nabla_x u) + G^{(y)}]_{y=\bar{u}+u(x)}\, dx.\end{aligned} \tag{2.26}$$

If ϕ is α-quasiperiodic and ψ is $(-\alpha)$-quasiperiodic, i.e.,

$$\phi(x+d,y) = e^{i\alpha\cdot d}\phi(x,y), \quad \psi(x+d,y) = e^{-i\alpha\cdot d}\psi(x,y), \tag{2.27}$$

then the Lemma 2.2 tells us, with $\mathbf{G} = (F^{(x)}, F^{(y)} + F^{(k)})^T$,

$$\begin{aligned}0 &= \int_\Omega Z^{(k)} dV = \int_{\partial\Omega} div[\mathbf{G}]dV \\ &= \int_0^d (F^{(x)} \cdot \nabla_x l - F^{(y)} - F^{(k)})_{y=\bar{l}+l(x)} dx \\ &+ \int_0^d (F^{(x)} \cdot (-\nabla_x u) + F^{(y)} + F^{(k)})_{y=\bar{u}+u(x)} dx,\end{aligned} \tag{2.28}$$

since, here, $F^{(x)}$, $F^{(y)}$, and $F^{(k)}$ are *periodic*. More specifically,

$$
\begin{aligned}
0 = \int_0^d & [\partial_y\psi(\nabla_x\psi\cdot\nabla_x l) + \nabla_x\phi\cdot(\partial_y\psi\nabla_x l) - \partial_y\phi(\partial_y\psi) \\
& + \nabla_x\phi\cdot(\nabla_x\psi) - k^2\phi\psi\, dx]_{y=\bar{l}+l(x)} \\
& + \int_0^d [\partial_y\phi(\nabla_x\psi\cdot(-\nabla_x u)) + \nabla_x\phi\cdot(\partial_y\psi\cdot(-\nabla_x u)) \\
& + \partial_y\phi(\partial_y\psi) - \nabla_x\phi\cdot(\nabla_x\psi) + k^2\phi\psi\, dx]_{y=\bar{u}+u(x)},
\end{aligned}
\tag{2.29}
$$

and

$$
\begin{aligned}
0 = & \int_0^d [\partial_y\psi(\nabla_x l\cdot\nabla_x\phi - \partial_y\psi) + \nabla_x\psi\cdot(\nabla_x l\partial_y\phi + \nabla_x\phi) - \psi k^2\phi]_{y=\bar{l}+l(x)}\, dx \\
& + \int_0^d [\partial_y\psi(-\nabla_x u\cdot\nabla_x\phi + \partial_y\phi) - \nabla_x\psi\cdot(\nabla_x u\partial_y\phi + \nabla_x\phi) + \psi k^2\phi]_{y=\bar{u}+u(x)}\, dx.
\end{aligned}
\tag{2.30}
$$

If we define

$$
\xi(x) := \phi(x, \bar{l} + l(x)), \quad \zeta(x) := \phi(x, \bar{u} + u(x)), \tag{2.31}
$$

then tangential derivatives are given by

$$\nabla_x\xi(x) := [\nabla_x\phi + \nabla_x l\partial_y\phi]_{y=\bar{l}+l(x)}, \quad \nabla_x\zeta(x) := [\nabla_x\phi + \nabla_x u\partial_y\phi]_{y=\bar{u}+u(x)}.$$

Normal derivatives are given by

$$L(x) := [-\partial_y\phi + \nabla_x l\cdot\nabla_x\phi]_{y=\bar{l}+l(x)}, \quad U(x) := [\partial_y\phi - \nabla_x u\cdot\nabla_x\phi]_{y=\bar{u}+u(x)},$$

which results in

$$
\begin{aligned}
0 = & \int_0^d (\partial_y\psi)_{y=\bar{l}+l(x)} L + (\nabla_x\psi)_{y=\bar{l}+l(x)}\cdot\nabla\xi - (\psi)_{y=\bar{l}+l(x)} k^2\xi\, dx \\
& + \int_0^d (\partial_y\psi)_{y=\bar{u}+u(x)} U - (\nabla_x\psi)_{y=\bar{u}+u(x)}\cdot\nabla_x\zeta + (\psi)_{y=\bar{u}+u(x)} k^2\zeta\, dx,
\end{aligned}
\tag{2.32}
$$

or

$$\begin{aligned}
&\int_0^d (\partial_y \psi)_{y=\bar{u}+u(x)} U + (\partial_y \psi)_{y=\bar{l}+l(x)} L \, dx \\
&= \int_0^d (\nabla_x \psi)_{y=\bar{u}+u(x)} \cdot \nabla_x \zeta \, dx - \int_0^d (\nabla_x \psi)_{y=\bar{l}+l(x)} \cdot \nabla_x \xi \, dx \\
&- \int_0^d k^2 (\psi)_{y=\bar{u}+u(x)} \zeta \, dx + \int_0^d k^2 (\psi)_{y=\bar{l}+l(x)} \xi \, dx.
\end{aligned} \tag{2.33}$$

2.4 The Top Layer

For this problem we consider upward propagating, α-quasiperiodic solutions of

$$\begin{aligned}
&\Delta \phi + k^2 \phi = 0, \quad && \bar{l} + l(x) < y < \bar{u} \\
&\phi = \xi, && y = \bar{l} + l(x).
\end{aligned}$$

To begin, we note that the Rayleigh expansion (39) gives, for $y > \bar{u}$, that upward propagating α-quasiperiodic solutions of the Helmholtz equation can be written as

$$\phi(x, y) = \sum_{q=-\infty}^{\infty} \hat{\zeta}_p e^{i\alpha_p \cdot x + i\beta_p (y - \bar{u})}, \quad p = (p_1, p_2), \quad p_1, p_2 \in \mathbb{Z}, \tag{2.34}$$

where

$$\alpha_p := \begin{pmatrix} \alpha_1 + 2\pi p_1 / d_1 \\ \alpha_2 + 2\pi p_2 / d_2 \end{pmatrix} \quad \beta_p := \begin{cases} \sqrt{(k)^2 - |\alpha_p^2|} & p \in \mathcal{U} \\ i\sqrt{|\alpha_p^2| - (k)^2} & p \notin \mathcal{U} \end{cases}, \tag{2.35}$$

and the set of propagating modes is specified by

$$\mathcal{U} := \{p \, | \, |\alpha_p|^2 < k^2\}.$$

Evaluating ϕ above at $y = \bar{u}$ delivers the (generalized) Fourier series of $\zeta(x)$,

$$\zeta(x) = \textstyle\sum_{p_1=-\infty}^{\infty} \sum_{p_2=-\infty}^{\infty} \hat{\zeta}_p e^{i\alpha_p \cdot x},$$

so that we can compute the DNO at $y = \bar{u}$ as

$$U = \partial_y \phi(x, \bar{u}) = \sum_{p_1=-\infty}^{\infty} \sum_{p_2=-\infty}^{\infty} (i\beta_p)\hat{\zeta}_p e^{i\alpha_p \cdot x} =: (i\beta_D)\zeta. \tag{2.36}$$

Proceeding, we consider an (-α)-quasiperiodic "test function"

$$\psi(x, y) = e^{-i\alpha_p \cdot x + im_p(y-\bar{l})}$$

with m_p to be determined so that the difference between the first and the sum of the third and fifth terms in (2.2) are zero. For this we consider the quantity

$$R(x) := (\partial_y \psi)_{y=\bar{u}} U - (\nabla_x \psi)_{y=\bar{u}} \cdot \nabla_x \zeta + k^2 (\psi)_{y=\bar{u}} \zeta,$$

and define

$$E_p := \exp(im_p(\bar{u} - \bar{l})).$$

It can be easily shown that

$$\begin{aligned} R(x) &= (im_p)e^{-i\alpha_p x} E_p (i\beta_D)\zeta - (-i\alpha_p)e^{-i\alpha_p x} E_p \cdot \nabla_x \zeta + k^2 e^{-i\alpha_p x} E_p \zeta \\ &= \sum_{q=-\infty}^{\infty} \{(im_p)(i\beta_q) - (-i\alpha_p) \cdot (i\alpha_p) + k^2\} E_p \hat{\zeta}_q e^{-i(\alpha_p - \alpha_q)\cdot x}. \end{aligned} \tag{2.37}$$

Integrating R over the period cell, the only non-zero term features $p = q$ so that

$$\int_0^d R(x)dx = |d|\{(im_p)(i\beta_p) - (-i\alpha_p) \cdot (i\alpha_p) + k^2\} E_p \hat{\zeta_p}.$$

Choosing $m_p = \beta_p$, so that

$$\psi(x, y) = e^{-i\alpha_p x + i\beta_p (y-\bar{l})},$$

a "conjugated solution," we get $\int_0^d R \, dx = 0$ since

$$\alpha_p \cdot \alpha_p + \beta_p^2 = k^2 \Rightarrow (i\alpha_p) \cdot (i\alpha_p) + (i\beta_p)^2 + k^2 = 0. \tag{2.38}$$

In light of these computations we now have

$$\int_0^d (\partial_y \psi)_{y=\bar{l}+l(x)} L\,dx = -\int_0^d (\nabla_x \psi)_{y=\bar{l}+l(x)} \cdot \nabla_x \xi\,dx + \int_o^d k^2 (\psi)_{y=\bar{l}+l(x)} \xi\,dx, \tag{2.39}$$

and, with ψ defined above,

$$\int_0^d (i\beta_p) e^{i\beta_p l} e^{-i\alpha_p x} L\,dx = -\int_0^d (-i\alpha_p) e^{i\beta_p l} e^{-i\alpha_p x} \cdot \nabla_x \xi\,dx + \int_0^d k^2 e^{i\beta_p l} e^{-i\alpha_p x} \xi\,dx. \tag{2.40}$$

2.5 The Bottom Layer

In a similar fashion we can consider downward propagating, α-quasiperiodic solutions of

$$\Delta\phi + k^2\phi = 0, \qquad \bar{l} < y < \bar{u} + u(x)$$
$$\phi = \zeta, \qquad y = \bar{u} + u(x),$$

and the "test function"

$$\psi(x, y) = e^{-i\alpha_p x - i\beta_p (y - \bar{u})}.$$

With this choice of ψ the second, fourth, and sixth terms in (2.34) combine to zero and we find

$$\int_0^d (\partial_y \psi)_{y=\bar{u}+u(x)} U\,dx = \int_0^d (\nabla_x \psi)_{y=\bar{u}+u(x)} \cdot \nabla_x \zeta\,dx - \int_0^d k^2 (\psi)_{y=\bar{u}+u(x)} \zeta\,dx. \tag{2.41}$$

With ψ defined in this way we determine that

$$\int_0^d (-i\beta_p)e^{-i\beta_p u}e^{-i\alpha_p x}U dx = \int_0^d (-i\alpha_p)e^{-i\beta_p u}e^{-i\alpha_p x}\cdot\nabla_x\zeta dx - \int_0^d k^2 e^{-i\beta_p u}e^{-i\alpha_p x}\zeta dx. \tag{2.42}$$

2.6 A Middle Layer

Finally, We consider α-quasiperiodic solutions of

$$\begin{aligned} &\Delta\phi + k^2\phi = 0, && \bar{l} + l(x) < y < \bar{u} + u(x) \\ &\phi = \xi, && y = \bar{l} + l(x) \\ &\phi = \zeta, && y = \bar{u} + u(x), \end{aligned}$$

and the "test functions"

$$\begin{aligned} \psi^{(u)}(x,y) &= \frac{\cosh(i\beta_p(y-\bar{l}))}{\sinh(i\beta_p(\bar{u}-\bar{l}))}e^{-i\alpha_p x} \\ \psi^{(l)}(x,y) &= \frac{\cosh(i\beta_p(\bar{u}-y))}{\sinh(i\beta_p(\bar{u}-\bar{l}))}e^{-i\alpha_p x}. \end{aligned} \tag{2.43}$$

Defining

$$\begin{aligned} co_p := \coth(i\beta_p(\bar{u}-\bar{l})), \quad cs_p := \operatorname{csch}(i\beta_p(\bar{u}-\bar{l})), \\ C(u) := \cosh(i\beta_p u), \quad S(u) := \sinh(i\beta_p u), \\ C(l) := \cosh(i\beta_p l), \quad S(l) := \sinh(i\beta_p l), \end{aligned} \tag{2.44}$$

we can show that

$$\begin{aligned}
\psi^{u}(x, \bar{u}+u) &= (co_p\, C(u) + S(u))e^{-i\alpha_p x} \\
\psi^{u}(x, \bar{l}+l) &= cs_p\, C(l)e^{-i\alpha_p x} \\
\psi^{l}(x, \bar{u}+u) &= cs_p\, C(u)e^{-i\alpha_p x} \\
\psi^{l}(x, \bar{l}+l) &= (co_p\, C(l) - S(l))e^{-i\alpha_p x},
\end{aligned} \tag{2.45}$$

and

$$\begin{aligned}
\partial_x\psi^{(u)}(x, \bar{u}+u) &= (-i\alpha_p)(co_p\, C(u) + S(u))e^{-i\alpha_p x} \\
\partial_x\psi^{(u)}(x, \bar{l}+l) &= (-i\alpha_p)\, cs_p\, C(l)e^{-i\alpha_p x} \\
\partial_x\psi^{(l)}(x, \bar{u}+u) &= (-i\alpha_p)\, cs_p\, C(u)e^{-i\alpha_p x} \\
\partial_x\psi^{(l)}(x, \bar{l}+l) &= (-i\alpha_p)(co_p\, C(l) - S(l))e^{-i\alpha_p x},
\end{aligned} \tag{2.46}$$

and

$$\begin{aligned}
\partial_y\psi^{(u)}(x, \bar{u}+u) &= (i\beta_p)(C(u) + co_p\, S(u))e^{-i\alpha_p x} \\
\partial_y\psi^{(u)}(x, \bar{l}+l) &= (i\beta_p)\, cs_p\, S(l)e^{-i\alpha_p x} \\
\partial_y\psi^{(l)}(x, \bar{u}+u) &= (i\beta_p)\, cs_p\, S(u)e^{-i\alpha_p x} \\
\partial_y\psi^{(l)}(x, \bar{l}+l) &= (-i\beta_p)(C(l) - co_p\, S(l))e^{-i\alpha_p x}.
\end{aligned} \tag{2.47}$$

From (2.34), with $\psi^{(u)}$ we find

$$\begin{aligned}
&\int_0^d (i\beta_p)(C(u) + co_p\, S(u))e^{-i\alpha_p x} U dx + \int_0^d (i\beta_p)\, cs_p\, S(l)e^{-i\alpha_p x} L dx \\
&\quad = \int_0^d (-i\alpha_p)(co_p C(u) + S(u))e^{-i\alpha_p x} \cdot \nabla_x \zeta dx - \int_0^d (-i\alpha_p) cs_p C(l) e^{-i\alpha_p x} \cdot \nabla_x \xi dx \quad (2.48) \\
&\quad \int_0^d k^2 cs_p C(l) e^{-i\alpha_p x} \xi dx - \int_0^d k^2 (co_p C(u) + S(u)) e^{-i\alpha_p x} \zeta dx.
\end{aligned}$$

With $\psi^{(l)}$ we find

$$\begin{aligned}
&\int_0^d (-i\beta_p)(C(l) - co_p S(l))e^{-i\alpha_p x} L dx + \int_0^d (i\beta_p) cs_p S(u) e^{-i\alpha_p x} U dx \\
&\quad = \int_0^d (-i\alpha_p)(co_p C(l) - S(l))e^{-i\alpha_p x} \cdot \nabla_x \xi dx + \int_0^d (-i\alpha_p) cs_p C(u) e^{-i\alpha_p x} \cdot \nabla_x \zeta dx \quad (2.49) \\
&\quad - \int_0^d k^2 cs_p C(u) e^{-i\alpha_p x} \zeta dx + \int_0^d k^2 (co_p C(l) - S(l)) e^{-i\alpha_p x} \xi dx.
\end{aligned}$$

2.7 Summary of Formulas and Zero-Deformation Simplifications

We point out that all of the formulas derived thus far, can be stated gererically as

$$\hat{A}_p[\tilde{V}] = \hat{R}_p[V]. \quad (2.50)$$

1. (Top Layer) For (2.43), after dividing by $(i\beta_p)$,

$$\tilde{V} = G, \quad V = \xi, \quad \hat{A}_p(g)[G] = \int_0^d e^{i\beta_p g} e^{-i\alpha_p x} G(x)\, dx, \quad (2.51)$$

and

$$\hat{R}_p(g)[\xi] = \int_0^d e^{i\beta_p g} e^{-i\alpha_p x} \frac{i\alpha_p}{i\beta_p} \cdot \nabla_x \xi(x) + \frac{k^2}{i\beta_p} \xi(x)\, dx. \quad (2.52)$$

2. (Bottom Layer) For (2.46), after dividing by $(i\beta_p)$

$$\tilde{V} = J, \quad V = \zeta, \quad \hat{A}_p(g)[J] = \int_0^d e^{i\beta_p g} e^{-i\alpha_p x} J(x)\, dx, \tag{2.53}$$

and

$$\hat{R}_p(g)[\zeta] = \int_0^d e^{i\beta_p g} e^{-i\alpha_p x} \frac{i\alpha_p}{i\beta_p} \cdot \nabla_x \zeta(x) + \frac{k^2}{i\beta_p} \zeta(x)\, dx. \tag{2.54}$$

3. (Middle Layer) For (2.52) and (2.53), after dividing by $(i\beta_p)$,

$$\tilde{V} = \begin{pmatrix} \tilde{V}^u \\ \tilde{V}^l \end{pmatrix} = \begin{pmatrix} U \\ L \end{pmatrix}, \quad V = \begin{pmatrix} V^u \\ V^l \end{pmatrix} = \quad \begin{pmatrix} \zeta \\ \xi \end{pmatrix}, \tag{2.55}$$

and

$$\hat{A}_p(u,l) \begin{pmatrix} U \\ L \end{pmatrix} = \int_0^d \begin{pmatrix} C(u) + co_p S(u) & cs_p S(l) \\ -cs_p S(u) & C(l) - co_p S(l) \end{pmatrix} \begin{pmatrix} U \\ L \end{pmatrix} e^{-i\alpha_p x} dx, \tag{2.56}$$

and

$$\begin{aligned} \hat{R}_p(u,l) \begin{pmatrix} \zeta \\ \xi \end{pmatrix} = \int_0^d & \begin{pmatrix} -S(u) - co_p C(u) & cs_p C(l) \\ cs_p C(u) & S(l) + co_p C(l) \end{pmatrix} \begin{pmatrix} U \\ L \end{pmatrix} \\ & (\frac{i\alpha_p}{i\beta_p} \cdot \nabla_x + \frac{k^2}{i\beta_p}) \begin{pmatrix} \zeta \\ \xi \end{pmatrix} e^{-i\alpha_p x} dx. \end{aligned} \tag{2.57}$$

In the case of flat interfaces ($g \equiv 0, u \equiv 0, l \equiv 0$) we have:

1. (Top Layer)

$$\hat{A}_p(0)[G] = \int_0^d e^{-i\alpha_p x} G(x)\, dx,$$
$$\hat{R}_p(0)[\xi] = \int_0^d e^{-i\alpha_p x} \{\frac{i\alpha_p}{i\beta_p} \cdot \nabla_x + \frac{k^2}{i\beta_p}\} \xi\, dx.$$

2. (Bottom Layer)

$$\hat{A}_p(0)[J] = \int_0^d e^{-i\alpha_p x} J(x)\, dx,$$
$$\hat{R}_p(0)[\zeta] = \int_0^d e^{-i\alpha_p x} \{\frac{i\alpha_p}{i\beta_p} \cdot \nabla_x + \frac{k^2}{i\beta_p}\} \zeta\, dx.$$

3. (Middle Layer)

$$\hat{A}_p(0,0) \begin{pmatrix} U \\ L \end{pmatrix} = \int_0^d \begin{pmatrix} 1 & 0 \\ 0 & 1 \end{pmatrix} \begin{pmatrix} U \\ L \end{pmatrix} e^{-i\alpha_p x}\, dx,$$
$$\hat{R}_p(0,0) \begin{pmatrix} \zeta \\ \xi \end{pmatrix} = \int_0^d \begin{pmatrix} -co_p & cs_p \\ cs_p & -co_p \end{pmatrix} \{\frac{i\alpha_p}{i\beta_p} \cdot \nabla_x + \frac{k^2}{i\beta_p}\} \begin{pmatrix} \zeta \\ \xi \end{pmatrix} e^{-i\alpha_p x}\, dx.$$

Recognizing the Fourier transform

$$\hat{\psi}_p = F[\psi] = \int_0^d e^{-i\alpha_p x} \psi dx,$$

and using the fact that $(i\alpha_p) \cdot (i\alpha_p) + k^2 = -(i\beta_p)^2$ we find:

1. (Top Layer)

$$\hat{A}_p(0)[G] = \hat{G}_p,$$
$$\hat{R}_p(0)[\xi] = \{\frac{i\alpha_p}{i\beta_p} \cdot (i\alpha_p) + \frac{k^2}{i\beta_p}\}\hat{\xi}_p = -(i\beta_p)\hat{\xi}_p.$$

2. (Bottom Layer)

$$\hat{A}_p(0)[J] = \hat{J}_p,$$
$$\hat{R}_p(0)[\zeta] = \{\frac{i\alpha_p}{i\beta_p} \cdot (i\alpha_p) + \frac{k^2}{i\beta_p}\}\hat{\zeta}_p = -(i\beta_p)\hat{\zeta}_p.$$

3. (Middle Layer)

$$\hat{A}_p(0,0)\begin{pmatrix} U \\ L \end{pmatrix} = \begin{pmatrix} 1 & 0 \\ 0 & 1 \end{pmatrix}\begin{pmatrix} \hat{U}_p \\ \hat{L}_p \end{pmatrix},$$
$$\hat{R}_p(0,0)\begin{pmatrix} \zeta \\ \xi \end{pmatrix} = \begin{pmatrix} -co_p & cs_p \\ cs_p & -co_p \end{pmatrix}\{\frac{i\alpha_p}{i\beta_p} \cdot (i\alpha_p) + \frac{k^2}{i\beta_p}\}\begin{pmatrix} \hat{\zeta}_p \\ \hat{\xi}_p \end{pmatrix}$$
$$= \begin{pmatrix} -co_p & cs_p \\ cs_p & -co_p \end{pmatrix}(-i\beta_p)\begin{pmatrix} \hat{\zeta}_p \\ \hat{\xi}_p, \end{pmatrix},$$

and discover the classical results:

$$\hat{G}_p = -(i\beta_p)\hat{\xi}_p, \quad \hat{J}_p = -(i\beta_p)\hat{\zeta}_p,$$

$$\begin{pmatrix} \hat{U}_p \\ \hat{L}_p \end{pmatrix} = (i\beta_p) \begin{pmatrix} -co_p & cs_p \\ cs_p & -co_p \end{pmatrix} \begin{pmatrix} \hat{\zeta}_p \\ \hat{\xi}_p \end{pmatrix}.$$

2.8 A High-Order Perturbation of Surfaces (HOPS) Method.

We recognize that these FIEs depend upon the boundary perturbation ($g = f(x)$) in a rather simple way. In fact, if we set $g(x) = \varepsilon f(x)$ then the integral operators $\hat{A}_p$ and $\hat{R}_p$ are *analytic* with respect to ε (sufficiently small)

$$\hat{A}_p(g) = \hat{A}_p(\varepsilon f) = \sum_{n=0}^{\infty} \hat{A}_{p,n}(f)\varepsilon^n, \quad \hat{R}_p(g) = \hat{R}_p(\varepsilon f) = \sum_{n=0}^{\infty} \hat{R}_{p,n}(f)\varepsilon^n. \tag{2.58}$$

In light of these expansions one can posit the forms

$$V(g) = V(\varepsilon f) = \sum_{n=0}^{\infty} V_n(f)\varepsilon^n, \quad \tilde{V}(g) = \tilde{V}(\varepsilon f) = \sum_{n=0}^{\infty} \tilde{V}_n(f)\varepsilon^n. \tag{2.59}$$

In particular, for the problem of computing a Dirichlet-Neumann Operator [28, 29, 30], given analytic Dirichlet data (so that the first expansion in (2.58) converges strongly), we fully anticipate that the corresponding Neumann data will also be analytic [28] so that the second expansion is also valid.

If we insert the expansions (2.58) and (2.59) into

$$\hat{A}_p[\tilde{V}] = \hat{R}_p[V], \quad p \in \mathbf{Z}, \tag{2.60}$$

this results in

$$\left(\sum_{n=0}^{\infty}\hat{A}_{p,n}\varepsilon^n\right)\left[\sum_{m=0}^{\infty}\tilde{V}_m\varepsilon^m\right]=\left(\sum_{n=0}^{\infty}\hat{R}_{p,n}\varepsilon^n\right)\left[\sum_{m=0}^{\infty}V_m\varepsilon^m\right]. \tag{2.61}$$

This, evidently regular, perturbation expansion can now be equated at successive orders of ϵ delivering,

$$\hat{A}_{p,0}[\tilde{V}_n]=\hat{R}_{p,0}[V_n]+\sum_{m=0}^{n-1}\hat{R}_{p,n-m}[V_m]-\sum_{m=0}^{n-1}\hat{A}_{p,n-m}[\tilde{V}_m]. \tag{2.62}$$

This recursion describes a natural HOPS scheme for the simulation of quantities of interest which is advantaged over (2.60) in a number of ways.

First, the solution of (2.60) requires the formation and inversion of $\hat{A}_p(g)$ which, as we shall show, can become quite *ill-conditioned* as the boundary deformation g departs significantly from zero. By contrast, in solving (2.61) one must (repeatedly) invert the operator $\hat{A}_{p,0}=\hat{A}_p(0)$ which, as we will see, is both *well-conditioned* and can be accomplished rapidly using the FFT algorithm.

Second, one may perceive that a disadvantage of utilizing (2.61) is that this system must be solved at every perturbation order n desired which would make it much more computationally intensive that inverting (2.60) once. However, this is, in fact, a *strength* as it allows one to compute the Neumann data for an entire *family* of profiles $g(x)=\epsilon f(x)$ with one simulation. That is, upon solving (2.61) for $0\leq n\leq N$ we can form

$$\tilde{V}^N(x;\varepsilon):=\sum_{n=0}^{N}\tilde{V}_n(x)\varepsilon^n, \tag{2.63}$$

and approximate $\tilde{V}$ corresponding to $g=\varepsilon f$ for any ε by a simple summation (with linear cost). By contrast, if one wished to do the same with (2.60), the operator $\hat{A}_p(g)$ must be formed and inverted with every new instance of g.

At this point we simply require forms for the Taylor coefficients of the integral operators $\hat{A}_p$ and $\hat{R}_p$, namely the $\{\hat{A}_{p,n}, \hat{R}_{p,n}\}$. As we now show, the matter is a simple one and in fact, in the previous section we identified the "flat interface" operators $\{\hat{A}_{p,0}, \hat{R}_{p,0}\}$ explicitly (though we made no particular use of them).

2.9 Higher-Order Corrections.

Based on the forms for (2.55 - 2.60), it is straightforward to compute the $\hat{A}_{p,n}$ and $\hat{R}_{p,n}$. In particular, for the upper layer, if $g(x) = \varepsilon f(x)$ then (2.54) gives

$$\hat{A}_{p,n}(f)[G] = \int_0^d (i\beta_p^{(0)})^n F_n(x) e^{-i\alpha_p \cdot x} G(x)\, dx, \tag{2.64}$$

and (2.55) gives

$$\hat{R}_{p,n}(f)[\xi] = \int_0^d (i\beta_p^{(0)})^n F_n(x) e^{-i\alpha_p \cdot x} \left\{ \frac{i\alpha_p}{i\beta_p^{(0)}} \cdot \nabla_x + \frac{(k^{(0)})^2}{i\beta_p^{(0)}} \right\} \xi(x)\, dx, \tag{2.65}$$

where $F_n(x) := f(x)^n/n!$. In the lower layer, if $g(x) = \varepsilon f(x)$ then (2.56) gives

$$\hat{A}_{p,n}(f)[J] = \int_0^d (-i\beta_p^{(M)})^n F_n(x) e^{-i\alpha_p \cdot x} J(x)\, dx, \tag{2.66}$$

and (2.57) gives

$$\hat{R}_{p,n}(f)[\zeta] = \int_0^d (i\beta_p^{(M)})^n F_n(x) e^{-i\alpha_p \cdot x} \left\{ \frac{i\alpha_p}{i\beta_p^{(M)}} \cdot \nabla_x + \frac{(k^{(M)})^2}{i\beta_p^{(M)}} \right\} \zeta(x)\, dx. \tag{2.67}$$

Finally, in a middle layer, if $u(x) = \varepsilon f_u(x)$ and $l(x) = \varepsilon f_l(x)$ then (2.59) gives

$$\hat{A}_{p,n}(f_u, f_l)\begin{pmatrix} U \\ L \end{pmatrix} = \int_0^d \begin{pmatrix} (C_n + co_p S_n)F_{u,n} & cs_p S_n F_{l,n} \\ -cs_p S_n F_{u,n} & (C_n - co_p S_n)F_{l,n} \end{pmatrix} \begin{pmatrix} U \\ L \end{pmatrix} e^{-i\alpha_p x}\, dx, \quad (2.68)$$

and

$$\begin{aligned} \hat{R}_{p,n}(f_u, f_l)\begin{pmatrix} \zeta \\ \xi \end{pmatrix} = \int_0^d & \begin{pmatrix} (-S_n - co_p C_n)F_{u,n} & cs_p C_n F_{l,n} \\ cs_p C_n F_{u,n} & (S_n - co_p C_n)F_{l,n} \end{pmatrix} \\ & \times \left\{ \frac{i\alpha_p}{i\beta_p^{(m)}} \cdot \nabla_x + \frac{(k^m)^2}{i\beta_p^{(m)}} \right\} \begin{pmatrix} \zeta \\ \xi \end{pmatrix} e^{-i\alpha_p x}\, dx, \end{aligned} \quad (2.69)$$

where,

$$F_{u,n} := (f_u(x))^n/n!, \quad F_{l,n} := (f_l(x))^n/n!,$$

and,

$$C_{2j} := (i\beta_p^m)^{2j}, \quad C_{2j+1} := 0, \quad S_{2j} := 0, \quad S_{2j+1} := (i\beta_p^m)^{2j+1}, \quad j = 0, 1, \ldots$$

At this point we are able to make a crucial observation which gives an unexpected computational benefit to our approach as opposed to the one advanced in previous section. Specifically, we note that in (2.64 - 2.69) we are able to separate the wavenumber (p) dependence from the spatial (x) dependence in the following ways. For (2.64) we write

$$\hat{A}_{p,n}(f)[G] = (i\beta_p^{(0)})^n \int_0^d F_n(x) e^{-i\alpha_p \cdot x} G(x)\, dx, \tag{2.70}$$

for (2.65)

$$\begin{aligned} \hat{R}_{p,n}(f)[\xi] = (i\beta_p^{(0)})^n \frac{i\alpha_p}{i\beta_p^{(0)}} \cdot \int_0^d F_n(x) e^{-i\alpha_p \cdot x} \nabla_x \xi(x) \\ + (i\beta_p^{(0)})^n \frac{(k^{(0)})^2}{i\beta_p^{(0)}} \int_0^d F_n(x) e^{-i\alpha_p \cdot x} \xi(x)\, dx, \end{aligned} \tag{2.71}$$

for (2.66)

$$\hat{A}_{p,n}(f)[J] = -(i\beta_p^{(M)})^n \int_0^d F_n(x) e^{-i\alpha_p \cdot x} J(x)\, dx, \tag{2.72}$$

and for (2.67)

$$\begin{aligned} \hat{R}_{p,n}(f)[\xi] = -(i\beta_p^{(M)})^n \frac{i\alpha_p}{i\beta_p^{(M)}} \cdot \int_0^d F_n(x) e^{-i\alpha_p \cdot x} \nabla_x \zeta(x) dx \\ + -(i\beta_p^{(M)})^n \frac{(k^{(M)})^2}{i\beta_p^{(M)}} \int_0^d F_n(x) e^{-i\alpha_p \cdot x} \zeta(x)\, dx. \end{aligned} \tag{2.73}$$

Finally, for (2.68 and 2.69) we get

$$\hat{A}_{p,n}(f_u, f_l) \begin{pmatrix} U \\ L \end{pmatrix} = \begin{pmatrix} (C_n + co_p S_n) & cs_p S_n \\ -cs_p S_n & (C_n - co_p S_n) \end{pmatrix} \int_0^d e^{-i\alpha_p \cdot x} \begin{pmatrix} F_{u,n} U \\ F_{l,n} L \end{pmatrix} dx, \tag{2.74}$$

$$\hat{R}_{p,n}(f_u, f_l)\begin{pmatrix}\zeta\\ \xi\end{pmatrix} = \begin{pmatrix}(-S_n - co_pC_n) & cs_pC_n\\ cs_pC_n & (S_n - co_pC_n)\end{pmatrix}\begin{pmatrix}i\alpha_p\\ i\beta_p^m\end{pmatrix}\cdot\int_0^d e^{-i\alpha_p\cdot x}\begin{pmatrix}F_{u,n}\nabla_x\zeta\\ F_{l,n}\nabla_x\xi\end{pmatrix}dx$$
$$+\begin{pmatrix}(-S_n - co_pC_n) & cs_pC_n\\ cs_pC_n & (S_n - co_pC_n)\end{pmatrix}\begin{pmatrix}(k^{(m)})^2\\ i\beta_p^m\end{pmatrix}\int_0^d e^{-i\alpha_p\cdot x}\begin{pmatrix}F_{u,n}\zeta\\ F_{l,n}\xi\end{pmatrix}dx. \tag{2.75}$$

The important observation to make about all of these is that they are convolution operators which can be rapidly evaluated by the FFT algorithm. For instance, in using (2.74 and 2.75) one could perform the following sequence of steps to evaluate the action of $\hat{A}_{n,p}$ on the function $G(x)$ evaluated at the N_x equally-spaced points on $[0, d]$:

1. Multiply $G(x)$ by $F_n(x)$ pointwise in "physical space" (Cost: $\mathcal{O}(N_x)$).
2. Fourier transform the product via the FFT (Cost: $\mathcal{O}(N_x log(N_x))$).
3. Multiply pointwise by the diagonal operator $(i\beta_p^{(0)})^n$ in "Fourier space" (Cost: $\mathcal{O}(N_x)$).

We point out that, at this point, it is quite natural to use inverse Fourier transform to move back to "physical space". We use this convention for the rest of this contribution which amounts to replacing (2.66) by

$$A_0[\tilde{V}_n] = R_0[V_n] + \sum_{m=0}^{n-1} R_{n-m}[V_m] - \sum_{m=0}^{n-1} A_{n-m}[\tilde{V}_m], \tag{2.76}$$

where

$$A_n = \frac{1}{|d|}\sum_{p=-\infty}^{\infty}\hat{A}_{p,n}e^{i\alpha_p\cdot\tilde{x}}, \quad R_n = \frac{1}{|d|}\sum_{p=-\infty}^{\infty}\hat{R}_{p,n}e^{i\alpha_p\cdot\tilde{x}}. \tag{2.77}$$

2.10 Exact Solutions

Unfortunately, there are no known exact solutions for plane-wave incidence for non-trivial interface shapes for the DNO problem. To prove that our algorithm converges we use the following principle: To build a numerical solver for

$$\begin{aligned} L\mathfrak{u} &= 0 \qquad \text{in } \Omega \\ B\mathfrak{u} &= 0 \qquad \text{at } \partial\Omega, \end{aligned} \tag{2.78}$$

it is often just as easy to create an algorithm for the corresponding *inhomogenous* problem:

$$\begin{aligned} L\mathfrak{u} &= \mathsf{R} \qquad \text{in } \Omega \\ B\mathfrak{u} &= \mathsf{Q} \qquad \text{at } \partial\Omega. \end{aligned} \tag{2.79}$$

Letting ω an arbitrary function, we can solve

$$\mathsf{R}_\omega := \mathsf{L}\omega, \quad \mathsf{Q}_\omega := \mathsf{B}\omega, \tag{2.80}$$

Using which we now have an $\mathtt{exact}$ solution for

$$\begin{aligned} L\mathfrak{u} &= \mathsf{R}_\omega \qquad \text{in } \Omega \\ B\mathfrak{u} &= \mathsf{Q}_\omega \qquad \text{at } \partial\Omega, \end{aligned} \tag{2.81}$$

namely $u = \omega$. Using this approach, we can test our homogenous solver which would be a special case ($R_\omega \equiv 0$) for our inhomogenous solver. We should however select ω which have the same "behavior" as solutions of u of the homogenous problem. Our exact solution however, does not correspond to plane-wave incidence rather plane-wave reflection.

To be specific, consider the family of functions

$$v_r^{(m)}(x,y) = A^{(m)} e^{i(\alpha_r \cdot x + \beta_r^{(m)} y)} + B^{(m)} e^{i(\alpha_r \cdot x - \beta_r^{(m)} y)}, \quad m \in \mathbb{Z} \tag{2.82}$$

with $A^{(M)} = B^{(0)} = 0$. and m denotes the surface layer. These are outgoing, α-quasiperiodic solutions of the Helmholtz equation, so that $R_\omega \equiv 0$ in the notation above. These functions however do not satisfy the boundary conditions satisfied by an incident plane wave. We compute the surface data with the construction of the Q_ω in mind

$$\tilde{\zeta}^{(m)} := v_r^{(m-1)} - v_r^{(m)} \qquad y = g(x),$$
$$\tilde{\psi}^{(m)} := \partial_{N^{(m)}}[v_r^{(m-1)} - v_r^{(m)}] \qquad y = g(x).$$

We test our numerical algorithm for any choice of deformation $g(x)$ using this family of exact solutions.

2.11 Numerical Implementation

We utilize Nyström's method (12) to simulate the Integral Equations (2.64) as they appear in $\mathbf{MV^l} = \mathbf{Q}$. In this setting this amounts to enforcing these equations at $N = (N_1, N_2)$ equally spaced gridpoints, $x_j = (x_{1,j_1}, x_{2,j_2})$, on the period cell $[0, d_1] \times [0, d_2]$, with unknowns being the functions $\tilde{V}^{(m),l}, V^{(m),l}$ at these same gridpoints x_j.

Using these we define,

$$\epsilon_{rel} := \sup_{0\le m\le M-1} \left\{ \frac{|\tilde{V}_r^{(m),l} - \tilde{V}_r^{(m),l,N}|_{L^\infty}}{|\tilde{V}_r^{(m),l}|_{L^\infty}}, \frac{|V_r^{(m),l} - V_r^{(m),l,N}|_{L^\infty}}{|V_r^{(m),l}|_{L^\infty}} \right\}. \tag{2.83}$$

2.12 Convergence Studies

For our convergence studies we follow the lead of (41) and select configurations quite close to the ones considered there. First, we consider the two-dimensional and 2ϕ-periodic profiles *independent* of the x_2- variable. We then consider the fully three-dimensional case. Recalling the three profiles introduced in (42): The sinusoid

$$f_s(x) = \cos(x) \tag{2.84}$$

the "rough" (C^4 but not C^5) profile

$$f_r(x) = (2\times 10^{-4}) \left\{ x^4(2\pi - x)^4 - \frac{128\pi^8}{315} \right\} \tag{2.85}$$

and the Lipschitz

$$f_L(x) = \begin{cases} -(2/\pi)x + 1, & 0 \le x \le \pi \\ (2/\pi)x - 3, & \pi \le x \le 2\pi \end{cases} \tag{2.86}$$

These profiles have approximate amplitude two, zero mean, and maximum slope of approximately one. The Fourier series of f_r and f_l are listed in (42). $f_{r,P}$ and $f_{L,P}$ represent the truncated P-term Fourier series.

We start with two three-layer configurations:

1. Two Smooth Interfaces

$$\begin{gathered}\alpha = 0.1, \quad \beta^{(0)} = 1.1, \quad \beta^{(1)} = 2.2, \quad \beta^{(2)} = 3.3, \\ g^{(1)}(x) = \epsilon f_s(x), \quad g^{(2)}(x) = \epsilon f_s(x), \quad \epsilon = 0.01, \quad d = 2\pi, \\ N = 10, ..., 30.\end{gathered} \tag{2.87}$$

2. Rough and Lipschitz Interfaces

$$\begin{gathered}\alpha = 0.1, \quad \beta^{(0)} = 1.1, \quad \beta^{(1)} = 2.2, \quad \beta^{(2)} = 3.3, \\ g^{(1)}(x) = \epsilon f_{r,40}(x), \quad g^{(2)}(x) = \epsilon f_{L,40}(x), \quad \epsilon = 0.03, \quad d = 2\pi, \\ N = 80, ..., 320.\end{gathered} \tag{2.88}$$

In these three-layer configurations the wavelengths of propagation ($\lambda^{(m)} = 2\pi/k^{(m)}$) are

$$\lambda^{(0)} \approx 5.6885, \quad \lambda^{(1)} \approx 2.8530, \quad \lambda^{(2)} \approx 1.9031. \tag{2.89}$$

In the first configuration, we show that only a small number of collocation points ($N \approx 20$) are sufficient to achieve machine precision for small, smooth profiles, (2.88), which displays the spectral accuracy of the scheme. In sumulation (2.92) provided that N is chosen sufficiently large, we show that the algorithm converges quickly even when smooth interfaces are replaced by the rough, (2.89), and Lispschitz, (2.90), profiles respectively (both truncated after $P = 4F0$ Fourier series terms).

Among the many multilayer configurations our algorithm can address we choose two more, representative ones:

1. Six-Layer

$$\begin{gathered}\alpha = 0.1, \quad \beta^{(m)} = 1.1 + m, \quad 0 \le m \le 5 \\ g^{(1)}(x) = \epsilon f_s(x), \quad g^{(2)}(x) = \epsilon f_{r,40}(x), \quad g^{(3)}(x) = \epsilon f_{L.40}(x), \\ g^{(4)}(x) = \epsilon f_{r,40}(x), \quad g^{(5)}(x) = \epsilon f_s(x), \epsilon = 0.02, \quad d = 2\pi, \\ N = 40, ..., 120.\end{gathered} \tag{2.90}$$

2. 21-Layer

$$\begin{gathered}\alpha = 0.1, \quad \beta^{(m)} = \frac{m+1}{10}, \quad 0 \le m \le 20 \\ g^{(m)}(x) = \epsilon f_s(x), 1 \le m \le 20, \quad \epsilon = 0.02, \quad d = 2\pi, \\ N = 10, ..., 30.\end{gathered} \tag{2.91}$$

We again show that in all cases, provided that a sufficient number of degrees of freedom are selected our algorithm provides highly accurate solutions in a stable and rapid manner.

We now consider $(2\pi) \times (2\pi)$ periodic interfaces in a three-dimensional structure. We select the following: The sinusoid

$$\tilde{f}_s(x_1, x_2) = \cos(x_1 + x_2), \tag{2.92}$$

the "rough" (C^2 but not C^3) profile

$$\tilde{f}_r(x_1, x_2) - \left(\frac{2}{9} \times 10^{-3}\right) \left\{x_1^2(2\pi - x_1)^2 x_2^2(2\pi - x_2)^2 - \frac{64\pi^8}{225}\right\}, \tag{2.93}$$

and the Lipschitz boundary

$$\tilde{f}_L(x_1,x_2)=\frac{1}{3}+\begin{cases}(2/\pi)x_1-1, & x_1\le x_2\le 2\pi-x_1\\ -(2/\pi)x_2+3, & x_2>x_1, x_2>2\pi-x_1\\ 3-(2/\pi)x_1, & 2\pi-x_1\le x_2\le x_1\\ -1+(2/\pi)x_2, & x_2<x_1, x_2<2\pi-x_1.\end{cases} \tag{2.94}$$

These profiles have approximate amplitude two, zero mean, and maximum slope of approximately one. The Fourier series of f_r and f_l are listed in (42). $f_{r,P}$ and $f_{L,P}$ represent the truncated P-term Fourier series.

We focus upon the two three-layer configurations outlined below.

1. Two Smooth Interfaces:

$$\begin{gathered}\alpha_1=0.1,\quad \alpha_2=0.2,\quad \beta^{(0)}=1.1,\quad \beta^{(1)}=2.2,\quad \beta^{(2)}=3.3,\\ g^{(1)}(x_1,x_2)=\epsilon\tilde{f}_s(x_1,x_2),\quad g^{(2)}(x_1,x_2)=\epsilon\tilde{f}_s(x_1,x_2),\quad \epsilon=0.1,\\ d_1=2\pi, d_2=2\pi,\quad N_1=N_2=6,...,32.\end{gathered} \tag{2.95}$$

2. Rough and Lipschitz interfaces:

$$\begin{gathered}\alpha_1=0.1,\quad \alpha_2=0.2,\quad \beta^{(0)}=1.1,\quad \beta^{(1)}=2.2,\quad \beta^{(2)}=3.3,\\ g^{(1)}(x_1.x_2)=\epsilon\tilde{f}_{r,20}(x_1,x_2),\quad g^{(2)}(x_1,x_2)=\epsilon\tilde{f}_{L,20}(x_1,x_2),\quad \epsilon=0.01,\\ d_1=2\pi, d_2=2\pi,\quad N_1=N_2=8,...,24.\end{gathered} \tag{2.96}$$

Our algorithm again delivers highly accurate results. Provided that a sufficient number of collocation points are used, our algorithm exhibits the same behavior independent of interface shape.

2.13 Layered Medium Simulation

Having verified the validity of our codes, we demonstrate the utility of our approach by simulating *plane-wave* scattering from all of the configurations described in the previous section. Recall, in two dimensions this included two-layer (2.91) & (2.92) and two multiple-layer problems (2.94) & (2.95); while in three dimensions this featured two two-layer scenarios (2.99) & (2.100). For this there is no exact solution for comparison we resort to the diagnostic of enery defect .

$$\delta = 1 - \sum_{p \in U^0} e_p^0 - \sum_{p \in U^M} e_p^M. \tag{2.97}$$

We observe in Figure 7 that we achieve full double precision accuracy with our coarsest discretization for the smooth-smooth configuration, (2.91), while in Figure 8 we show that the same can be realized with $N \approx 200$ for the rough-Lipschitz problem, (2.92). The same generic behavior is noticed for the six-layer configuration, (2.94), and the 21 layer device, (2.95), which are displayed in Figures 9 and 10, respectively. Finally, we display three-dimensional results corresponding to the two-layer problems, (2.99) & (2.100), and the quantitative results are given in Figures 11 & 12, respectively.

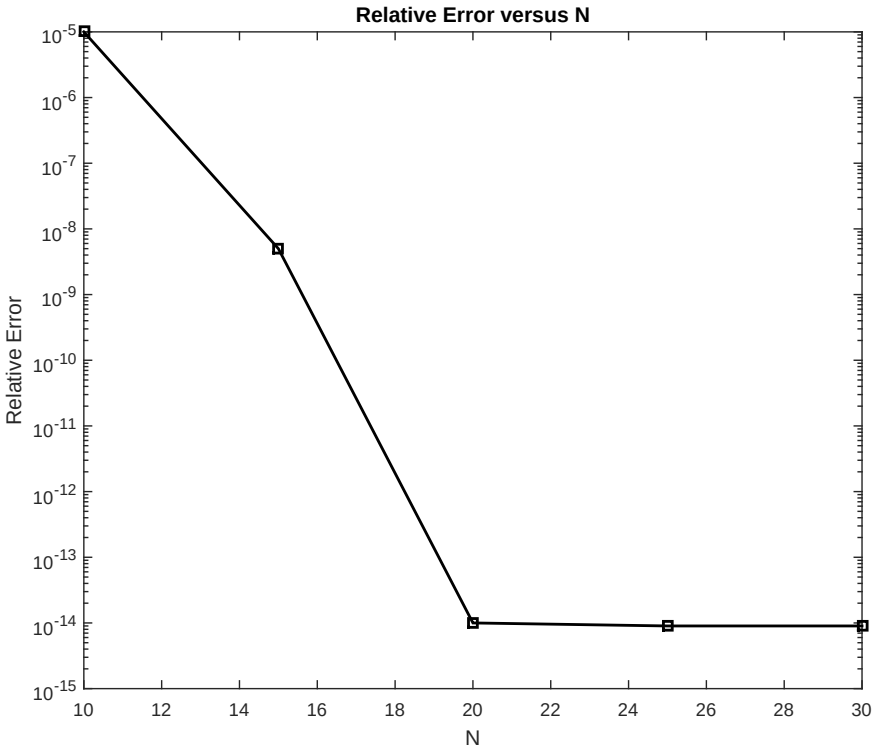

Figure 1. Relative error for 2D smooth-smooth config (Eq: 2.91) for Helmholtz equation

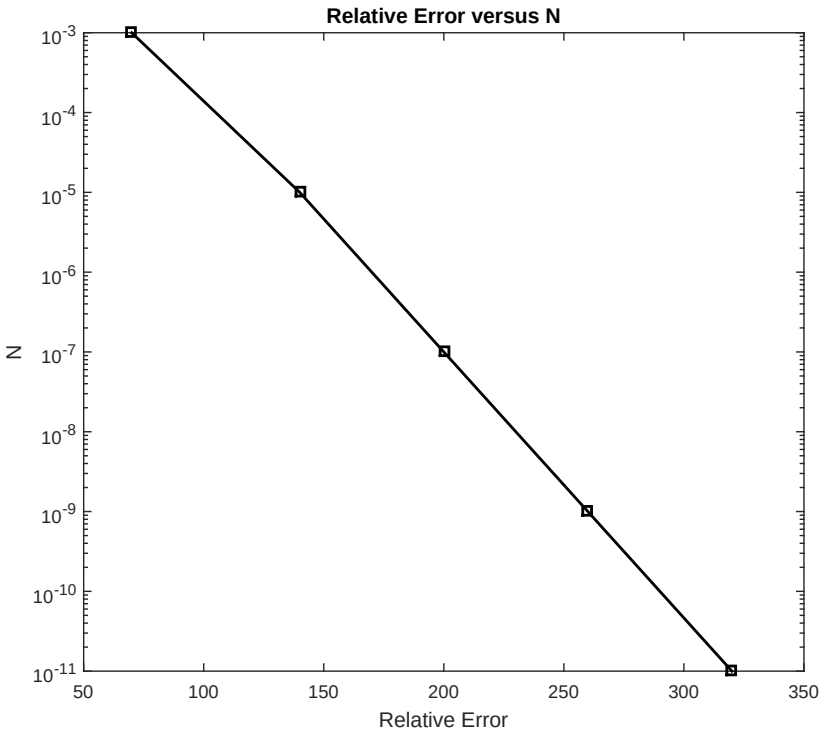

Figure 2. Relative error for 2D rough-Lipschitz config (Eq: 2.92) for Helmholtz equation

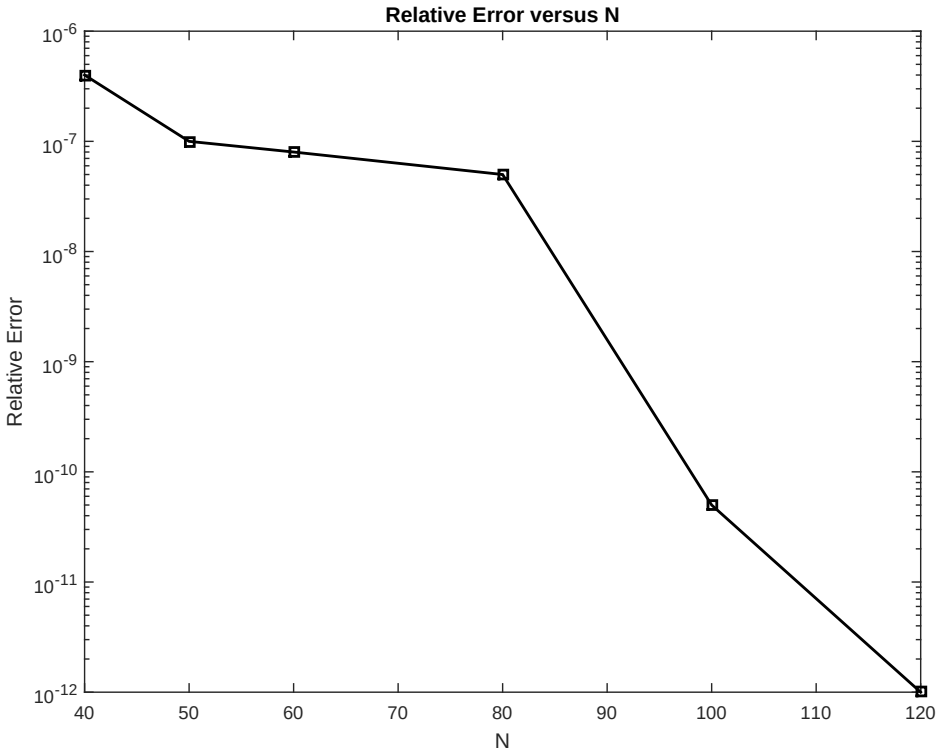

Figure 3. Relative error for 2D smooth- rough-Lipschitz-rough-smooth config (Eq: 2.94) for Helmholtz equation

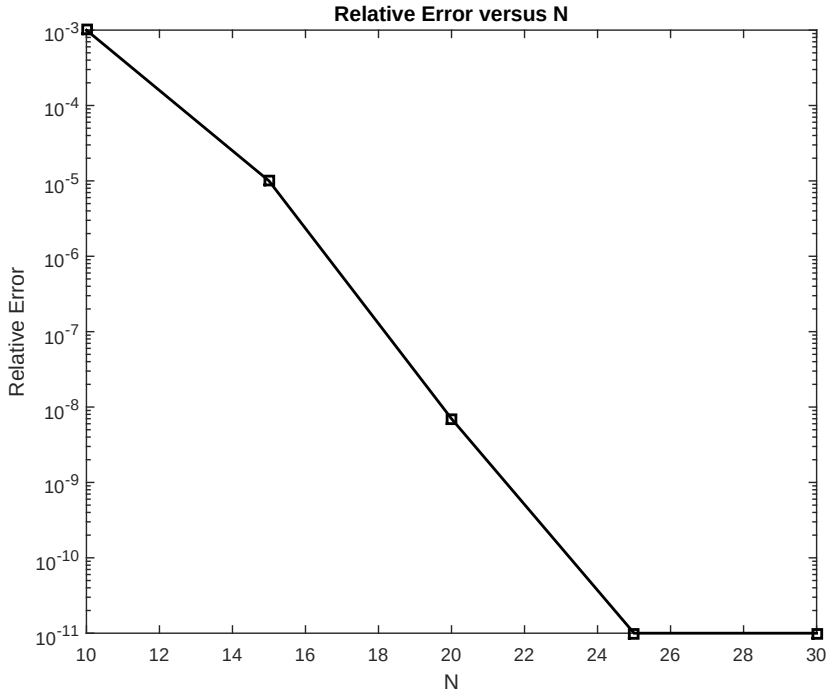

Figure 4. Relative error for 20 smooth interfaces (Eq: 2.95) for Helmholtz equation

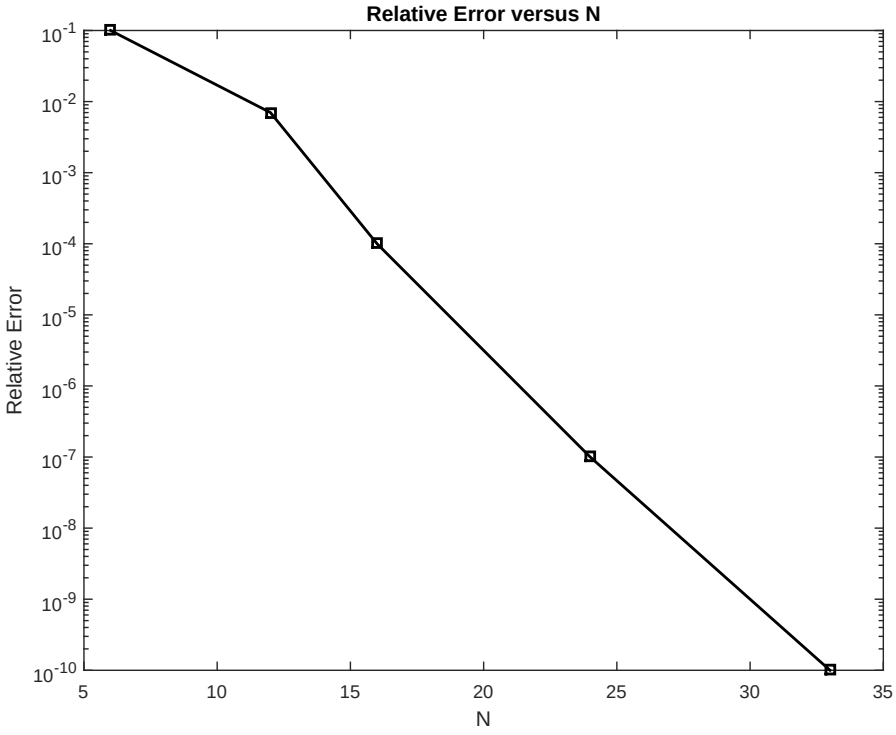

Figure 5. Relative error for 3D smooth-smooth configuration (Eq: 2.99) for Helmholtz equation

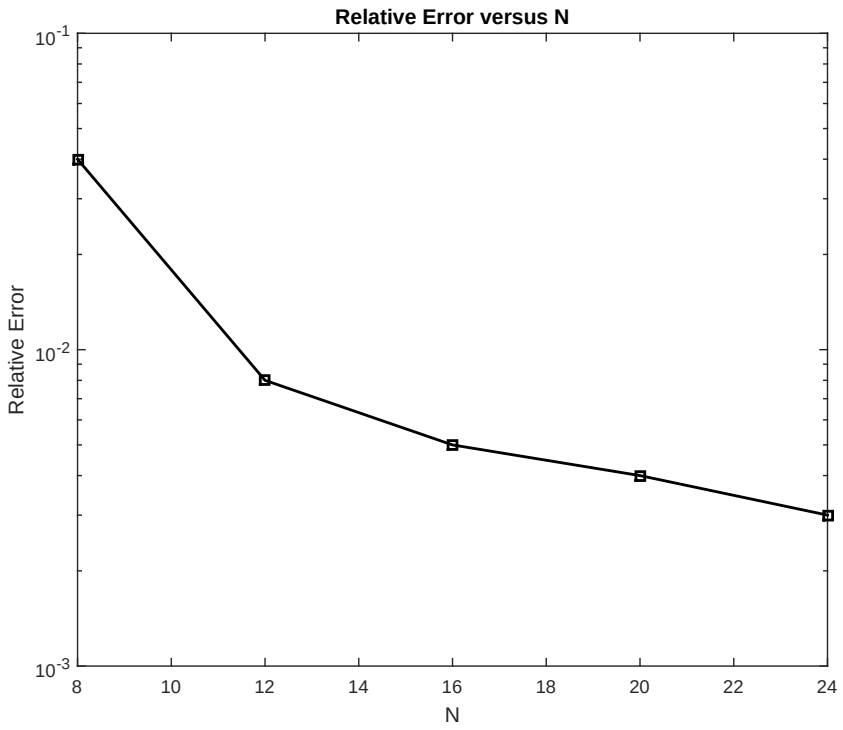

Figure 6. Relative error for 3D rough-Lipschitz configuration (Eq: 2.100) for Helmholtz equation

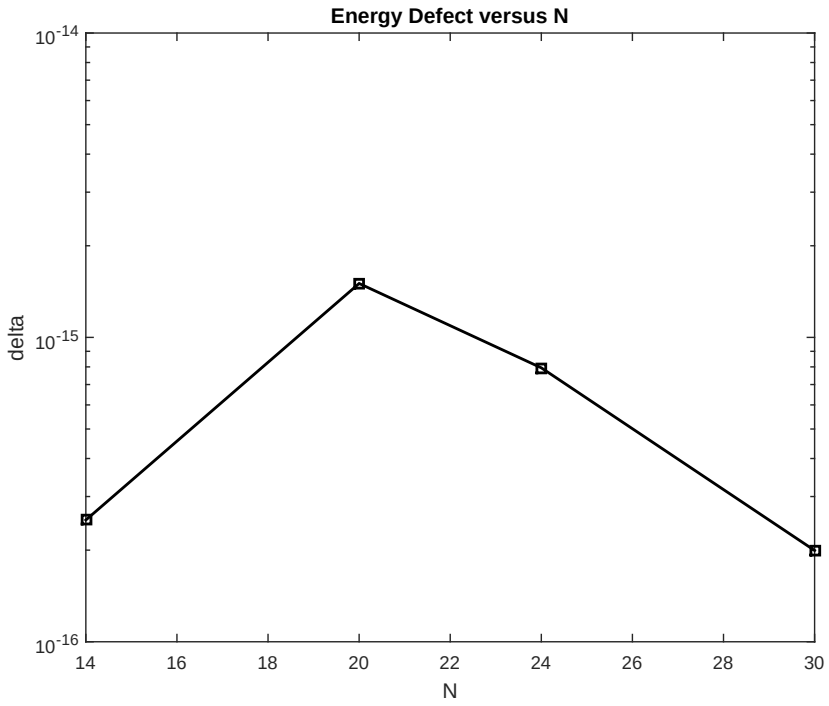

Figure 7. Energy defect for 2D smooth-smooth configuration (Eq: 2.91) for Helmholtz equation

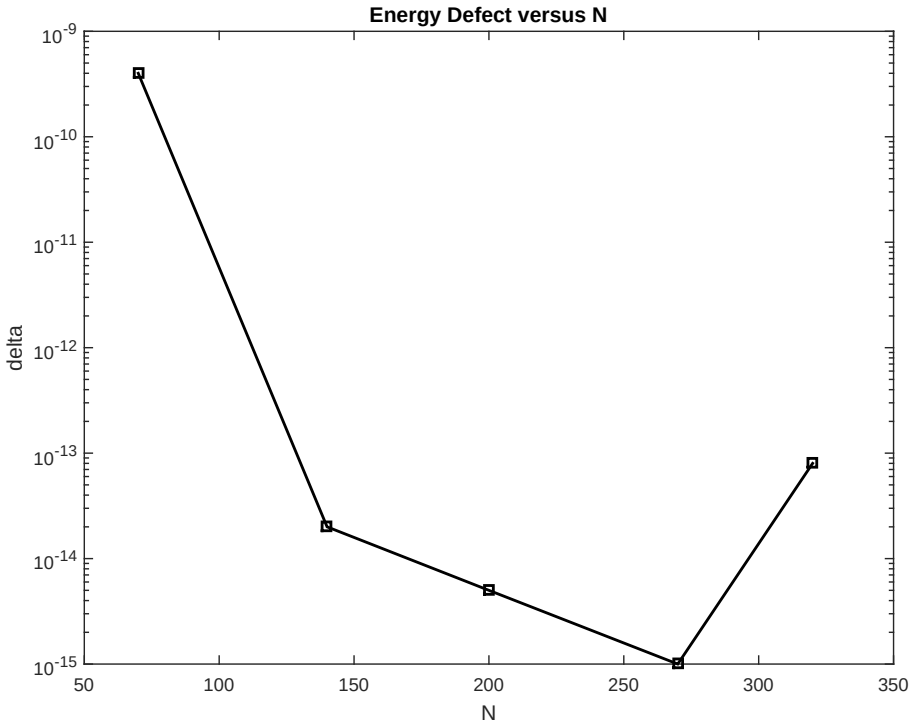

Figure 8. Energy defect for 2D rough-Lipschitz configuration (Eq: 2.92) for Helmholtz equation

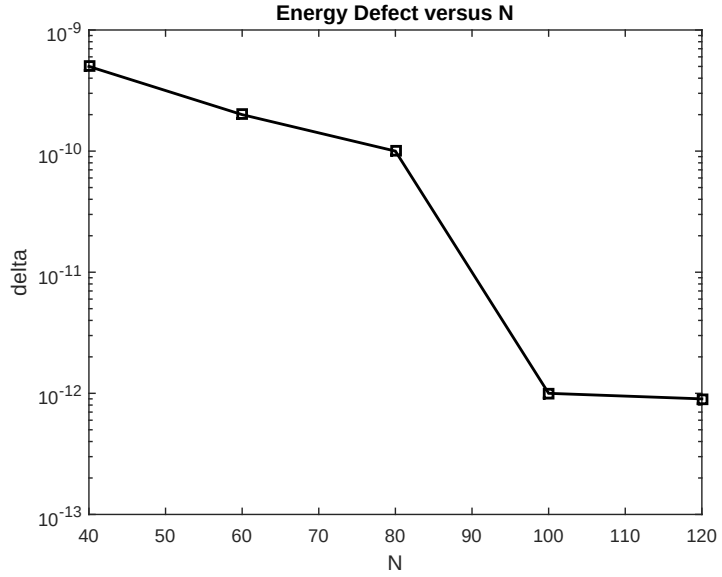

Figure 9. Energy defect for 2D smooth-rough-Lipschitz-rough-smooth config (Eq: 2.94) for Helmholtz equation

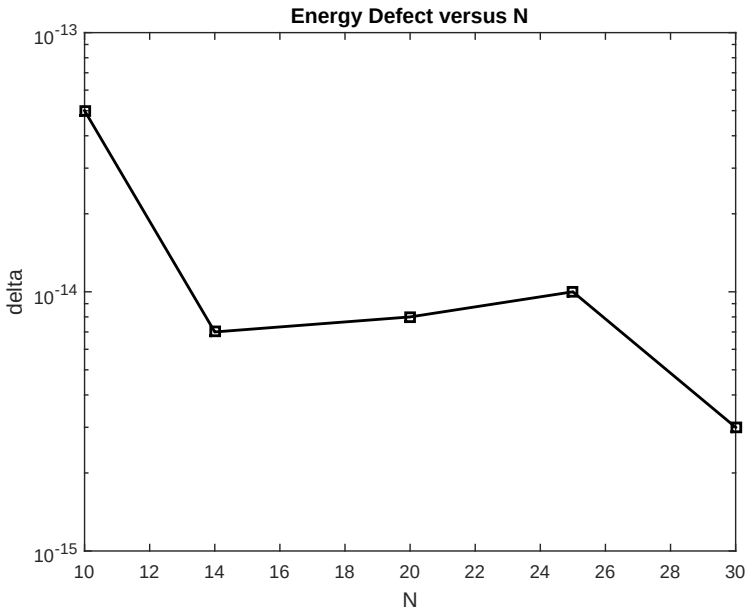

Figure 10. Energy defect for 21 layer config with 20 smooth interfaces (Eq: 2.95) for Helmholtz equation

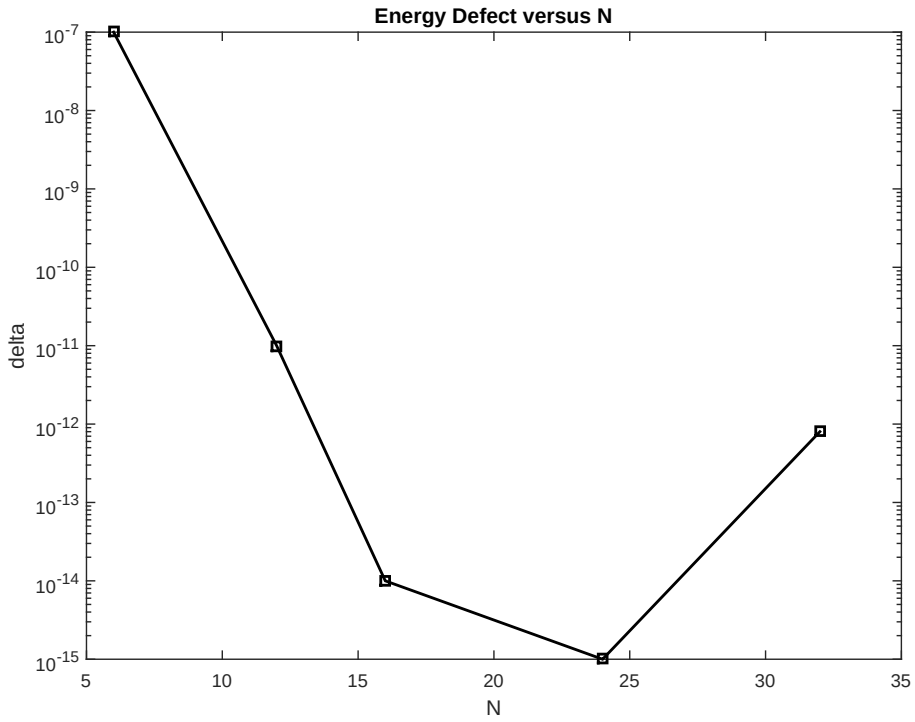

Figure 11. Energy defect for 3D smooth-smooth configuration (Eq: 2.99) for Helmholtz equation

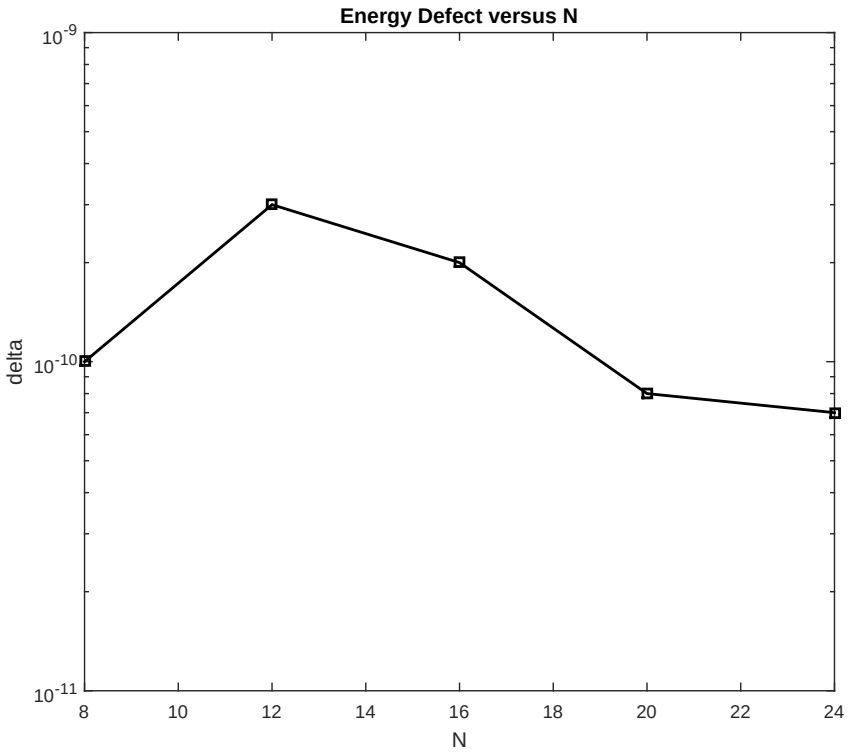

Figure 12. Energy defect for 3D smooth-smooth configuration (Eq: 2.100) for Helmholtz equation

CHAPTER 3

THREE DIMENSIONAL SCATTERING: THE MAXWELL EQUATION

3.1 The Governing Equations

At $z = g(x, y)$, lets consider a diffraction grating with crossed periodic interface.

Where x and y are the lateral coordinates, and z is the vertical coordinate.

The inteface delineates two layers

$$S^+ := \{z > g(x, y)\}, \quad S^- := \{z < g(x, y)\}.$$

The layers are filled with materials having dielectric constants $\{\epsilon^u, \epsilon^w\}$, permeability of each equal to μ_0. In this chapter we consider the *crossed* and periodic grating interface

$$g(x + d_1, y + d_2) = g(x, y);$$

see Figure Figure 13. Figure 3.1: Plot of the configuration with grating interface shaped by $g(x, y) = (\varepsilon/4)\,(\cos(2\pi x/d_1) + \cos(2\pi y/d_2))$, $d_1 = d_2 = d = 500$ nm, $\varepsilon/d = 0.01$ giving $\varepsilon = 5$ nm.

The plane–wave incidence is of the form

$$\mathbf{E}^{inc}(x, y, z) := e^{i\omega t}\underline{\mathbf{E}}^{inc}(x, y, z, t) = \mathbf{A}e^{i(\alpha x+\beta y-\gamma z)}$$

$$\mathbf{H}^{inc}(x, y, z) := e^{i\omega t}\underline{\mathbf{H}}^{inc}(x, y, z, t) = \mathbf{B}e^{i(\alpha x+\beta y-\gamma z)},$$

where

$$\mathbf{A} \cdot \kappa = 0, \quad \mathbf{B} = \frac{1}{\omega\mu_0}\kappa \times \mathbf{A}, \quad |\mathbf{A}| = |\mathbf{B}| = 1,$$

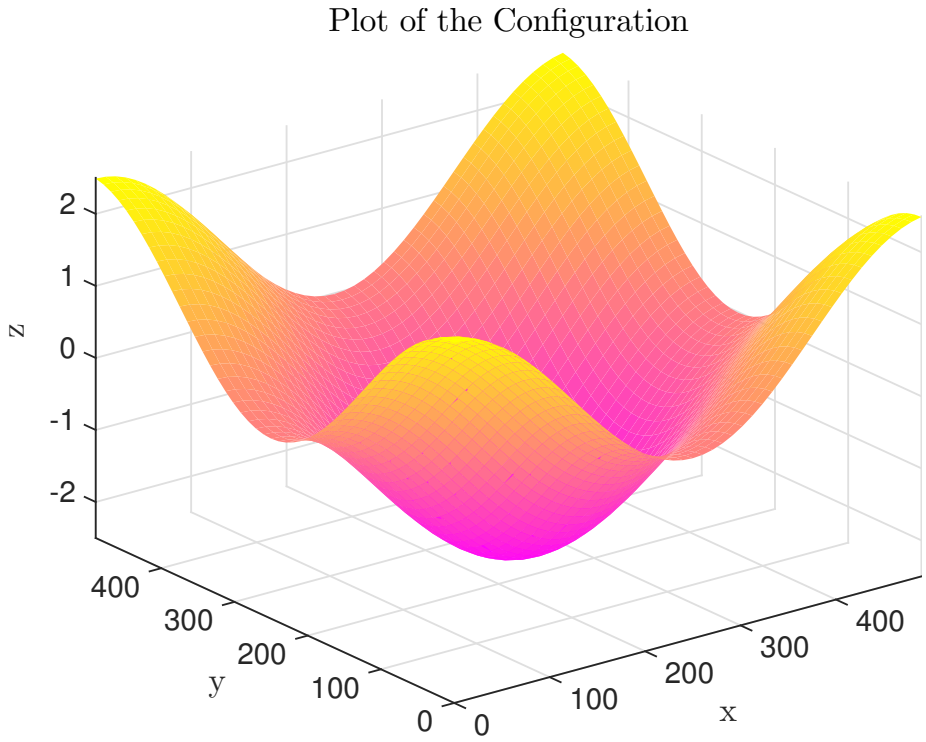

Figure 13. Configuration Plot for Maxwell problem

and $\kappa := (\alpha, \beta, -\gamma)^T$.

As before dropping the factor $\exp(-i\omega t)$, the time–harmonic Maxwell equations (43; 39) can be written as

$$\nabla \times \mathbf{E} = i\omega\mu_0\mathbf{H}, \quad \operatorname{div}[\mathbf{E}] = 0, \tag{3.1a}$$

$$\nabla \times \mathbf{H} = -i\omega\varepsilon\mathbf{E}, \quad \operatorname{div}[\mathbf{H}] = 0. \tag{3.1b}$$

All the reduced fields satisfy the vector Helmholtz equation, e.g.,

$$\Delta\mathbf{E} + k^2\mathbf{E} = 0, \tag{3.2}$$

with $k^2 = \omega^2\varepsilon\mu_0$.

The total fields are decomposed into incident and scattered components by

$$\mathbf{E} = \begin{cases} \mathbf{E}^u + \mathbf{E}^{inc} & \text{in } S^u \\ \mathbf{E}^w & \text{in } S^w \end{cases}, \quad \mathbf{H} = \begin{cases} \mathbf{H}^u + \mathbf{H}^{inc} & \text{in } S^u \\ \mathbf{H}^w & \text{in } S^w \end{cases},$$

and each satisfy vector Helmholtz equations, e.g.,

$$\Delta \mathbf{E}^u + (k^u)^2 \mathbf{E}^u = 0, \quad \text{in } S^u$$

where $(k^u)^2 := \omega^2 \varepsilon^u \mu_0$, and

$$\alpha^2 + \beta^2 + \gamma^2 = (k^u)^2.$$

At the interface, the transmission conditions (43; 39),

$$N \times [\mathbf{E}^u - \mathbf{E}^w] = \zeta$$

$$N \times [\mathbf{H}^u - \mathbf{H}^w] = \psi,$$

where $N := (-\partial_x g, -\partial_y g, 1)^T$, and,

$$\zeta = -N \times \left[\mathbf{E}^{inc}\right]_{z=g}, \quad \psi = -N \times \left[\mathbf{H}^{inc}\right]_{z=g}.$$

In light of Maxwell's equations, (Equation 3.1), we get

$$N \times [\mathbf{E}^u - \mathbf{E}^w]_{z=g} = \zeta, \tag{3.3a}$$

$$N \times [\nabla \times [\mathbf{E}^u - \mathbf{E}^w]]_{z=g} = \psi, \tag{3.3b}$$

where

$$\psi = -N \times \left[\nabla \times \left[\mathbf{E}^{inc}\right]\right]_{z=g}.$$

We point out that only four of these six boundary conditions are linearly dependent (the z–component of each can be written as a linear combination of the x– and y–components, for instance). Clearly it only makes sense to enforce four and we choose the x– and y–components of each. To compensate for this "defect" we recall that the electric field is divergence free in the bulk, and must also be so at the interface. Thus we enforce the two additional boundary conditions

$$\operatorname{div}[\mathbf{E}^u] = \operatorname{div}[\mathbf{E}^w] = 0, \quad z = g. \tag{3.3c}$$

Finally, the fields are quasiperiodic because of the periodicity of the grating interfaces

$$\mathbf{E}^m(x + d_1, y + d_2, z) = e^{i(\alpha d_1 + \beta d_2)}\mathbf{E}^m(x, y, z), \quad m = u, w,$$

and we demand that $\mathbf{E}^u$ and $\mathbf{E}^w$ are outgoing at positive and negative infinity, respectively.

3.2 The Rayleigh Expansions, Efficiencies, and the Reflectivity Map

Rayleigh expansions (39) which are quasiperiodic, outgoing solutions of (Equation 3.2) are given by separation of variables. The electric fields can be expanded as

$$\mathbf{E}^u(x, y, z) = \sum_{p=-\infty}^{\infty} \sum_{q=-\infty}^{\infty} \mathbf{a}_{p,q} e^{i\gamma^u_{p,q} z} e^{i(\alpha_p x + \beta_q y)} \tag{3.4a}$$

and

$$\mathbf{E}^w(x, y, z) = \sum_{p=-\infty}^{\infty} \sum_{q=-\infty}^{\infty} \mathbf{d}_{p,q} e^{-i\gamma^w_{p,q} z} e^{i(\alpha_p x + \beta_q y)}, \tag{3.4b}$$

where, for $p, q \in \mathbb{Z}$,

$$\alpha_p := \alpha + (2\pi/d_1)p, \quad \beta_q := \beta + (2\pi/d_2)q,$$

$$\gamma^m_{p,q} := \begin{cases} \sqrt{(k^m)^2 - \alpha_p^2 - \beta_q^2} & (p, q) \in \mathcal{U}^m \\ i\sqrt{\alpha_p^2 + \beta_q^2 - (k^m)^2} & (p, q) \notin \mathcal{U}^m \end{cases}, \quad m = u, w,$$

and,

$$\mathcal{U}^m = \left\{ p, q \in \mathbb{Z} \mid \alpha_p^2 + \beta_q^2 < (k^m)^2 \right\}, \quad m = u, w,$$

which are the "propagating modes" in the upper and lower layers. (Where $\mathbf{a}_{p,q}$ and $\mathbf{d}_{p,q}$ are the upward and downward propagating Rayleigh amplitudes.) *Efficiencies* are given by

$$e_{p,q}^u = (\gamma_{p,q}^u/\gamma) \left|\mathbf{a}_{p,q}\right|^2, \qquad (p, q) \in \mathcal{U}^u,$$

$$e_{p,q}^w = (\gamma_{p,q}^w/\gamma) \left|\mathbf{d}_{p,q}\right|^2, \qquad (p, q) \in \mathcal{U}^w,$$

and the object of fundamental importance to the design of Surface Plasmon Resonance (SPR) biosensors (44; 45; 46; 47; 48; 49) is the "Reflectivity Map"

$$R := \sum_{(p,q) \in \mathcal{U}^u} e_{p,q}^u. \tag{3.5}$$

If the lower layer is filled with a perfect electric conductor, and a lossless dielectric fills the upper medium, we get $R = 1$ by conservation of energy. However in the case of a metal (such as gold) in the lower domain, R drops in its value to a tenth or even a hundredth. This is the fundamental phenomenon behind the utility of Surface Plasmon Resonance (SPR) sensors (50; 51; 52).

3.3 Boundary Formulation

We will now demonstrate how the governing equations (Equation 3.2) & (Equation 3.3) can be rewritten in terms of surface quantities, more specifically the Dirichlet and (exterior) Neumann traces. For this we define the surface quantities

$$\mathbf{U}(x, y) := \mathbf{E}^u(x, y, g(x, y)) \tag{3.6a}$$

$$\mathbf{W}(x, y) := \mathbf{E}^w(x, y, g(x, y)) \tag{3.6b}$$

$$\tilde{\mathbf{U}}(x, y) := \left[-\partial_z \mathbf{E}^u + (\partial_x g)\partial_x \mathbf{E}^u + (\partial_y g)\partial_y \mathbf{E}^u\right](x, y, g(x, y)) \tag{3.6c}$$

$$\tilde{\mathbf{W}}(x, y) := \left[\partial_z \mathbf{E}^w - (\partial_x g)\partial_x \mathbf{E}^w - (\partial_y g)\partial_y \mathbf{E}^w\right](x, y, g(x, y)), \tag{3.6d}$$

where

$$\mathbf{U} = \begin{pmatrix} U^x \\ U^y \\ U^z \end{pmatrix}, \quad \mathbf{W} = \begin{pmatrix} W^x \\ W^y \\ W^z \end{pmatrix}, \quad \tilde{\mathbf{U}} = \begin{pmatrix} \tilde{U}^x \\ \tilde{U}^y \\ \tilde{U}^z \end{pmatrix}, \quad \tilde{\mathbf{W}} = \begin{pmatrix} \tilde{W}^x \\ \tilde{W}^y \\ \tilde{W}^z \end{pmatrix},$$

so

$$\left\{\mathbf{U}, \mathbf{W}, \tilde{\mathbf{U}}, \tilde{\mathbf{W}}\right\} : \mathbf{R}^2 \to \mathbf{R}^3,$$
$$\left\{U^j, W^j, \tilde{U}^j, \tilde{W}^j\right\} : \mathbf{R}^2 \to \mathbf{R}, \qquad j = x, y, z.$$

As each of the components of $\{\mathbf{U}, \mathbf{W}\}$ is an outgoing, quasiperiodic solution of the Helmholtz equation, (Equation 3.2), the Dirichlet and Neumann traces are related by the Fokas Integral Equations (FIE) (16; 17)

$$A^u \tilde{U}^j - R^u U^j = 0, \quad A^w \tilde{W}^j - R^w W^j = 0, \quad j = x, y, z. \tag{3.7}$$

The operators are defined (for $j = x, y, z$) by

$$A^u[\tilde{U}^j] := \frac{1}{d_1 d_2} \sum_{p=-\infty}^{\infty} \sum_{q=-\infty}^{\infty} \hat{A}^u_{p,q}[\tilde{U}^j] e^{i(\alpha_p x + \beta_q y)},$$
$$R^u[U^j] := \frac{1}{d_1 d_2} \sum_{p=-\infty}^{\infty} \sum_{q=-\infty}^{\infty} \hat{R}^u_{p,q}[U^j] e^{i(\alpha_p x + \beta_q y)},$$

and

$$A^w[\tilde{W}^j] := \frac{1}{d_1 d_2} \sum_{p=-\infty}^{\infty} \sum_{q=-\infty}^{\infty} \hat{A}^w_{p,q}[\tilde{W}^j] e^{i(\alpha_p x + \beta_q y)},$$
$$R^w[W^j] := \frac{1}{d_1 d_2} \sum_{p=-\infty}^{\infty} \sum_{q=-\infty}^{\infty} \hat{R}^w_{p,q}[W^j] e^{i(\alpha_p x + \beta_q y)}.$$

In these

$$\hat{A}^{u}_{p,q}[\tilde{U}] := \int_0^{d_1}\int_0^{d_2} e^{i\gamma^{u}_{p,q}g(x,y)}e^{-i(\alpha_p x+\beta_q y)}\tilde{U}(x,y)\,dx\,dy$$
$$\hat{R}^{u}_{p,q}[U] := \int_0^{d_1}\int_0^{d_2} e^{i\gamma^{u}_{p,q}g(x,y)}e^{-i(\alpha_p x+\beta_q y)}\left\{\frac{i\alpha_p\partial_x + i\beta_q\partial_y + (k^u)^2}{i\gamma^{u}_{p,q}}\right\}U(x,y)\,dx\,dy$$
$$\hat{A}^{w}_{p,q}[\tilde{W}] := \int_0^{d_1}\int_0^{d_2} e^{-i\gamma^{w}_{p,q}g(x,y)}e^{-i(\alpha_p x+\beta_q y)}\tilde{W}(x,y)\,dx\,dy$$
$$\hat{R}^{w}_{p,q}[W] := \int_0^{d_1}\int_0^{d_2} e^{-i\gamma^{w}_{p,q}g(x,y)}e^{-i(\alpha_p x+\beta_q y)}\left\{\frac{i\alpha_p\partial_x + i\beta_q\partial_y + (k^w)^2}{i\gamma^{w}_{p,q}}\right\}W(x,y)\,dx\,dy.$$

3.4 Tangential Trace

Regarding the boundary conditions, we begin with the trace of the tangential component of a vector field. For this we have

$$N \times \mathbf{U} = S\mathbf{U},$$

where

$$S := \begin{pmatrix} 0 & -1 & -(\partial_y g) \\ 1 & 0 & (\partial_x g) \\ (\partial_y g) & -(\partial_x g) & 0 \end{pmatrix}.$$

We further require the (x,y)–projection operator

$$P_{x,y}\mathbf{U} = P_{x,y}\begin{pmatrix} U^x \\ U^y \\ U^z \end{pmatrix} = \begin{pmatrix} U^x \\ U^y \end{pmatrix},$$

so that

$$P_{x,y} := \begin{pmatrix} 1 & 0 & 0 \\ 0 & 1 & 0 \end{pmatrix}.$$

This gives

$$S_{x,y} := P_{x,y}S = \begin{pmatrix} S^{xx} & S^{xy} & S^{xz} \\ S^{yx} & S^{yy} & S^{yz} \end{pmatrix},$$

where

$$S^{xx} = 0, \quad S^{xy} = -1, \quad S^{xz} = -(\partial_y g), \quad S^{yx} = 1, \quad S^{yy} = 0, \quad S^{yz} = (\partial_x g). \tag{3.8}$$

Thus, the two (x– and y–components of the) Dirichlet boundary conditions, (Equation 3.3a), read

$$S_{x,y}\mathbf{U} - S_{x,y}\mathbf{W} = P_{x,y}\zeta. \tag{3.9}$$

3.5 Tangential Curl

We recall that the curl of $\mathbf{E}^m$ is given by

$$\nabla \times \mathbf{E}^m = \begin{pmatrix} \partial_y E^{m,z} - \partial_z E^{m,y} \\ \partial_z E^{m,x} - \partial_x E^{m,z} \\ \partial_x E^{m,y} - \partial_y E^{m,x} \end{pmatrix}, \quad m = u, w.$$

We now change to the surface variables $\{\mathbf{U}, \mathbf{W}\}$ with tangential derivatives $\{(\partial_x \mathbf{U}, \partial_y \mathbf{U}), (\partial_x \mathbf{W}, \partial_y \mathbf{W})\}$, and normal derivatives, $\{\tilde{\mathbf{U}}, \tilde{\mathbf{W}}\}$. The chain rule gives

$$\begin{aligned}
\partial_x \mathbf{U}(x,y) &= [\partial_x \mathbf{E}^u + (\partial_x g)\partial_z \mathbf{E}^u](x, y, g(x,y)), \\
\partial_y \mathbf{U}(x,y) &= [\partial_y \mathbf{E}^u + (\partial_y g)\partial_z \mathbf{E}^u](x, y, g(x,y)), \\
\partial_x \mathbf{W}(x,y) &= [\partial_x \mathbf{E}^w + (\partial_x g)\partial_z \mathbf{E}^w](x, y, g(x,y)), \\
\partial_y \mathbf{W}(x,y) &= [\partial_y \mathbf{E}^w + (\partial_y g)\partial_z \mathbf{E}^w](x, y, g(x,y)),
\end{aligned}$$

while (Equation 3.6) gives formulas for $\tilde{\mathbf{U}}$ and $\tilde{\mathbf{W}}$. It is not difficult to see that

$$\begin{aligned}
|N|^2 \partial_x \mathbf{E}^u &= \left(|N|^2 - (\partial_x g)^2\right) \partial_x \mathbf{U} - (\partial_x g)(\partial_y g)\partial_y \mathbf{U} + (\partial_x g)\tilde{\mathbf{U}} \\
|N|^2 \partial_y \mathbf{E}^u &= -(\partial_x g)(\partial_y g)\partial_x \mathbf{U} + \left(|N|^2 - (\partial_y g)^2\right) \partial_y \mathbf{U} + (\partial_y g)\tilde{\mathbf{U}} \\
|N|^2 \partial_z \mathbf{E}^u &= (\partial_x g)\partial_x \mathbf{U} + (\partial_y g)\partial_y \mathbf{U} - \tilde{\mathbf{U}},
\end{aligned}$$

and

$$
\begin{aligned}
|N|^2\,\partial_x \mathbf{E}^w &= \left(|N|^2 - (\partial_x g)^2\right)\partial_x \mathbf{W} - (\partial_x g)(\partial_y g)\partial_y \mathbf{W} - (\partial_x g)\tilde{\mathbf{W}} \\
|N|^2\,\partial_y \mathbf{E}^w &= -(\partial_x g)(\partial_y g)\partial_x \mathbf{W} + \left(|N|^2 - (\partial_y g)^2\right)\partial_y \mathbf{W} - (\partial_y g)\tilde{\mathbf{W}} \\
|N|^2\,\partial_z \mathbf{E}^w &= (\partial_x g)\partial_x \mathbf{W} + (\partial_y g)\partial_y \mathbf{W} + \tilde{\mathbf{W}},
\end{aligned}
$$

where

$$
|N|^2 = (\partial_x g)^2 + (\partial_y g)^2 + 1.
$$

In light of this inconvenient pre–factor, regarding the tangential curl boundary condition, (Equation 3.3b), we premultiply by $|N|^2$ and enforce the equivalent equation

$$
N \times \left[|N|^2\,\nabla \times [\mathbf{E}^u - \mathbf{E}^w]\right]_{z=g} = |N|^2\,\psi. \tag{3.10}
$$

Regarding the curl of $\mathbf{E}^u$ we now proceed deliberately, beginning with the x–component

$$
\begin{aligned}
|N|^2\,(\partial_y E^{u,z} - \partial_z E^{u,y}) &= \left\{-(\partial_x g)(\partial_y g)\partial_x U^z + \left(|N|^2 - (\partial_y g)^2\right)\partial_y U^z + (\partial_y g)\tilde{U}^z\right\} \\
&\quad - \left\{(\partial_x g)\partial_x U^y + (\partial_y g)\partial_x U^y - \tilde{U}^y\right\} \\
&= \tilde{C}^{u,xx}\tilde{U}^x + \tilde{C}^{u,xy}\tilde{U}^y + \tilde{C}^{u,xz}\tilde{U}^z + C^{u,xx}U^x + C^{u,xy}U^y + C^{u,xz}U^z,
\end{aligned}
$$

where

$$\tilde{C}^{u,xx} = 0, \tag{3.11a}$$

$$\tilde{C}^{u,xy} = 1, \tag{3.11b}$$

$$\tilde{C}^{u,xz} = (\partial_y g), \tag{3.11c}$$

$$C^{u,xx} = 0, \tag{3.11d}$$

$$C^{u,xy} = -(\partial_x g)\partial_x - (\partial_y g)\partial_y, \tag{3.11e}$$

$$C^{u,xz} = -(\partial_x g)(\partial_y g)\partial_x + \left(|N|^2 - (\partial_y g)^2\right)\partial_y. \tag{3.11f}$$

Continuing, for the y–component,

$$\begin{aligned}
|N|^2\left(\partial_z E^{u,x} - \partial_x E^{u,z}\right) &= \left\{(\partial_x g)\partial_x U^x + (\partial_y g)\partial_y U^x - \tilde{U}^x\right\} \\
&\quad - \left\{\left(|N|^2 - (\partial_x g)^2\right)\partial_x U^z - (\partial_x g)(\partial_y g)\partial_y U^z + (\partial_x g)\tilde{U}^z\right\} \\
&= \tilde{C}^{u,yx}\tilde{U}^x + \tilde{C}^{u,yy}\tilde{U}^y + \tilde{C}^{u,yz}\tilde{U}^z + C^{u,yx}U^x + C^{u,yy}U^y + C^{u,yz}U^z,
\end{aligned}$$

where

$$\tilde{C}^{u,yx} = -1, \tag{3.12a}$$

$$\tilde{C}^{u,yy} = 0, \tag{3.12b}$$

$$\tilde{C}^{u,yz} = -(\partial_x g), \tag{3.12c}$$

$$C^{u,yx} = (\partial_x g)\partial_x + (\partial_y g)\partial_y, \tag{3.12d}$$

$$C^{u,yy} = 0, \tag{3.12e}$$

$$C^{u,yz} = -\left(|N|^2 - (\partial_x g)^2\right)\partial_x + (\partial_x g)(\partial_y g)\partial_y. \tag{3.12f}$$

Finally, for the z–component,

$$\begin{aligned}|N|^2\left(\partial_x E^{u,y}-\partial_y E^{u,x}\right) &= \left\{\left(|N|^2-(\partial_x g)^2\right)\partial_x U^y-(\partial_x g)(\partial_y g)\partial_y U^y+(\partial_x g)\tilde{U}^y\right\}\\ &\quad-\left\{-(\partial_x g)(\partial_y g)\partial_x U^x+\left(|N|^2-(\partial_y g)^2\right)\partial_y U^x+(\partial_y g)\tilde{U}^x\right\}\\ &= \tilde{C}^{u,zx}\tilde{U}^x+\tilde{C}^{u,zy}\tilde{U}^y+\tilde{C}^{u,zz}\tilde{U}^z+C^{u,zx}U^x+C^{u,zy}U^y+C^{u,zz}U^z,\end{aligned}$$

where

$$\tilde{C}^{u,zx} = -(\partial_y g), \tag{3.13a}$$

$$\tilde{C}^{u,zy} = (\partial_x g), \tag{3.13b}$$

$$\tilde{C}^{u,zz} = 0, \tag{3.13c}$$

$$C^{u,zx} = (\partial_x g)(\partial_y g)\partial_x - \left(|N|^2-(\partial_y g)^2\right)\partial_y, \tag{3.13d}$$

$$C^{u,zy} = \left(|N|^2-(\partial_x g)^2\right)\partial_x - (\partial_x g)(\partial_y g)\partial_y, \tag{3.13e}$$

$$C^{u,zz} = 0. \tag{3.13f}$$

Defining

$$\tilde{C}^u = \begin{pmatrix}\tilde{C}^{u,xx} & \tilde{C}^{u,xy} & \tilde{C}^{u,xz}\\ \tilde{C}^{u,yx} & \tilde{C}^{u,yy} & \tilde{C}^{u,yz}\\ \tilde{C}^{u,zx} & \tilde{C}^{u,zy} & \tilde{C}^{u,zz}\end{pmatrix}, \quad C^u = \begin{pmatrix}C^{u,xx} & C^{u,xy} & C^{u,xz}\\ C^{u,yx} & C^{u,yy} & C^{u,yz}\\ C^{u,zx} & C^{u,zy} & C^{u,zz}\end{pmatrix},$$

we have

$$|N|^2\,\nabla\times\mathbf{E}^u = \begin{pmatrix}\tilde{C}^u & C^u\end{pmatrix}\begin{pmatrix}\tilde{\mathbf{U}}\\ \mathbf{U}\end{pmatrix}.$$

Again considering that we only wish to enforce these for the x– and y–components, we define

$$C^{u}_{x,y} := S_{x,y} C^{u} = \begin{pmatrix} -C^{u,yx} - (\partial_y g) C^{u,zx} & -C^{u,yy} - (\partial_y g) C^{u,zy} & -C^{u,yz} - (\partial_y g) C^{u,zz} \\ C^{u,xx} + (\partial_x g) C^{u,zx} & C^{u,xy} + (\partial_x g) C^{u,zy} & C^{u,xz} + (\partial_x g) C^{u,zz} \end{pmatrix}$$

$$\tilde{C}^{u}_{x,y} := S_{x,y} \tilde{C}^{u} = \begin{pmatrix} -\tilde{C}^{u,yx} - (\partial_y g) \tilde{C}^{u,zx} & -\tilde{C}^{u,yy} - (\partial_y g) \tilde{C}^{u,zy} & -\tilde{C}^{u,yz} - (\partial_y g) \tilde{C}^{u,zz} \\ \tilde{C}^{u,xx} + (\partial_x g) \tilde{C}^{u,zx} & \tilde{C}^{u,xy} + (\partial_x g) \tilde{C}^{u,zy} & \tilde{C}^{u,xz} + (\partial_x g) \tilde{C}^{u,zz} \end{pmatrix}.$$

In an analogous manner one can derive for the curl of $\mathbf{E}^{w}$ that

$$|N|^2 \nabla \times \mathbf{E}^{u} = \begin{pmatrix} \tilde{C}^{w} & C^{w} \end{pmatrix} \begin{pmatrix} \tilde{\mathbf{U}} \\ \mathbf{U} \end{pmatrix},$$

where

$$\tilde{C}^{w} = \begin{pmatrix} \tilde{C}^{w,xx} & \tilde{C}^{w,xy} & \tilde{C}^{w,xz} \\ \tilde{C}^{w,yx} & \tilde{C}^{w,yy} & \tilde{C}^{w,yz} \\ \tilde{C}^{w,zx} & \tilde{C}^{w,zy} & \tilde{C}^{w,zz} \end{pmatrix}, \quad C^{w} = \begin{pmatrix} C^{w,xx} & C^{w,xy} & C^{w,xz} \\ C^{w,yx} & C^{w,yy} & C^{w,yz} \\ C^{w,zx} & C^{w,zy} & C^{w,zz} \end{pmatrix}.$$

As before we define

$$C^{w}_{x,y} := S_{x,y} C^{w} = \begin{pmatrix} -C^{w,yx} - (\partial_y g) C^{w,zx} & -C^{w,yy} - (\partial_y g) C^{w,zy} & -C^{w,yz} - (\partial_y g) C^{w,zz} \\ C^{w,xx} + (\partial_x g) C^{w,zx} & C^{w,xy} + (\partial_x g) C^{w,zy} & C^{w,xz} + (\partial_x g) C^{w,zz} \end{pmatrix}$$

$$\tilde{C}^{w}_{x,y} := S_{x,y} \tilde{C}^{w} = \begin{pmatrix} -\tilde{C}^{w,yx} - (\partial_y g) \tilde{C}^{w,zx} & -\tilde{C}^{w,yy} - (\partial_y g) \tilde{C}^{w,zy} & -\tilde{C}^{w,yz} - (\partial_y g) \tilde{C}^{w,zz} \\ \tilde{C}^{w,xx} + (\partial_x g) \tilde{C}^{w,zx} & \tilde{C}^{w,xy} + (\partial_x g) \tilde{C}^{w,zy} & \tilde{C}^{w,xz} + (\partial_x g) \tilde{C}^{w,zz} \end{pmatrix},$$

so that the (x– and y–components of the) two Neumann boundary conditions, (Equation 3.10), read

$$\tilde{C}^{u}_{x,y} \tilde{\mathbf{U}} + C^{u}_{x,y} \mathbf{U} - \tilde{C}^{w}_{x,y} \tilde{\mathbf{W}} - C^{w}_{x,y} \mathbf{W} = P_{x,y} |N|^2 \psi. \tag{3.14}$$

The entries of these operators can be shown to be

$$\tilde{C}^{w,xx} = 0, \tag{3.15a}$$

$$\tilde{C}^{w,xy} = -1, \tag{3.15b}$$

$$\tilde{C}^{w,xz} = -(\partial_y g), \tag{3.15c}$$

$$C^{w,xx} = 0, \tag{3.15d}$$

$$C^{w,xy} = -(\partial_x g)\partial_x - (\partial_y g)\partial_y, \tag{3.15e}$$

$$C^{w,xz} = -(\partial_x g)(\partial_y g)\partial_x + \left(|N|^2 - (\partial_y g)^2\right)\partial_y, \tag{3.15f}$$

and

$$\tilde{C}^{w,yx} = 1, \tag{3.16a}$$

$$\tilde{C}^{w,yy} = 0, \tag{3.16b}$$

$$\tilde{C}^{w,yz} = (\partial_x g), \tag{3.16c}$$

$$C^{w,yx} = (\partial_x g)\partial_x + (\partial_y g)\partial_y, \tag{3.16d}$$

$$C^{w,yy} = 0, \tag{3.16e}$$

$$C^{w,yz} = -\left(|N|^2 - (\partial_y g)^2\right)\partial_x + (\partial_x g)(\partial_y g)\partial_y, \tag{3.16f}$$

and

$$\tilde{C}^{w,zx} = (\partial_y g), \tag{3.17a}$$

$$\tilde{C}^{w,zy} = -(\partial_x g), \tag{3.17b}$$

$$\tilde{C}^{w,zz} = 0, \tag{3.17c}$$

$$C^{w,zx} = (\partial_x g)(\partial_y g)\partial_x - \left(|N|^2 - (\partial_y g)^2\right)\partial_y, \tag{3.17d}$$

$$C^{w,zy} = \left(|N|^2 - (\partial_x g)^2\right)\partial_x - (\partial_x g)(\partial_y g)\partial_y, \tag{3.17e}$$

$$C^{w,zz} = 0. \tag{3.17f}$$

3.6 Divergence–Free Conditions

Finally, we enforce the divergence–free condition (again premultiplied by the factor $|N|^2$) in the new variables

$$\begin{aligned}
|N|^2 \operatorname{div}[\mathbf{E}^u] &= |N|^2 \left(\partial_x E^{u,x} + \partial_y E^{u,y} + \partial_z E^{u,z}\right) \\
&= \left(|N|^2 - (\partial_x g)^2\right) \partial_x U^x - (\partial_x g)(\partial_y g)\partial_y U^x + (\partial_x g)\tilde{U}^x \\
&\quad + -(\partial_x g)(\partial_y g)\partial_x U^y + \left(|N|^2 - (\partial_y g)^2\right) \partial_y U^y + (\partial_y g)\tilde{U}^y \\
&\quad + (\partial_x g)\partial_x U^z + (\partial_y g)\partial_y U^z - \tilde{U}^z \\
&= \tilde{D}^{u,x}\tilde{U}^x + \tilde{D}^{u,y}\tilde{U}^y + \tilde{D}^{u,z}\tilde{U}^z + D^{u,x}U^x + D^{u,y}U^y + D^{u,z}U^z,
\end{aligned}$$

where,

$$\tilde{D}^{u,x} = (\partial_x g), \tag{3.18a}$$

$$\tilde{D}^{u,y} = (\partial_y g), \tag{3.18b}$$

$$\tilde{D}^{u,z} = -1, \tag{3.18c}$$

$$D^{u,x} = \left(|N|^2 - (\partial_x g)^2\right) \partial_x - (\partial_x g)(\partial_y g)\partial_y, \tag{3.18d}$$

$$D^{u,y} = -(\partial_x g)(\partial_y g)\partial_x + \left(|N|^2 - (\partial_y g)^2\right) \partial_y, \tag{3.18e}$$

$$D^{u,z} = (\partial_x g)\partial_x + (\partial_y g)\partial_y. \tag{3.18f}$$

In a similar manner,

$$\begin{aligned}
|N|^2 \operatorname{div}[\mathbf{E}^w] &= |N|^2 \left(\partial_x E^{w,x} + \partial_y E^{w,y} + \partial_z E^{w,z}\right) \\
&= \tilde{D}^{w,x}\tilde{W}^x + \tilde{D}^{w,y}\tilde{W}^y + \tilde{D}^{w,z}\tilde{W}^z + D^{w,x}W^x + D^{w,y}W^y + D^{w,z}W^z,
\end{aligned}$$

where

$$\tilde{D}^{w,x} = -(\partial_x g), \tag{3.19a}$$

$$\tilde{D}^{w,y} = -(\partial_y g), \tag{3.19b}$$

$$\tilde{D}^{w,z} = 1, \tag{3.19c}$$

$$D^{w,x} = \left(|N|^2 - (\partial_x g)^2\right)\partial_x - (\partial_x g)(\partial_y g)\partial_y, \tag{3.19d}$$

$$D^{w,y} = -(\partial_x g)(\partial_y g)\partial_x + \left(|N|^2 - (\partial_y g)^2\right)\partial_y, \tag{3.19e}$$

$$D^{w,z} = (\partial_x g)\partial_x + (\partial_y g)\partial_y. \tag{3.19f}$$

If we define

$$\tilde{D}^u := \begin{pmatrix} \tilde{D}^{u,x} & \tilde{D}^{u,y} & \tilde{D}^{u,z} \end{pmatrix}, \quad D^u := \begin{pmatrix} D^{u,x} & D^{u,y} & D^{u,z} \end{pmatrix},$$
$$\tilde{D}^w := \begin{pmatrix} \tilde{D}^{w,x} & \tilde{D}^{w,y} & \tilde{D}^{w,z} \end{pmatrix}, \quad D^w := \begin{pmatrix} D^{w,x} & D^{w,y} & D^{w,z} \end{pmatrix},$$

then the two divergence–free conditions read

$$\begin{pmatrix} \tilde{D}^u & D^u \end{pmatrix} \begin{pmatrix} \tilde{\mathbf{U}} \\ \mathbf{U} \end{pmatrix} = 0, \quad \begin{pmatrix} \tilde{D}^w & D^w \end{pmatrix} \begin{pmatrix} \tilde{\mathbf{W}} \\ \mathbf{W} \end{pmatrix} = 0. \tag{3.20}$$

3.7 Surface Equations

Summarizing all of these developments, we find that we must solve (Equation 3.7), (Equation 3.9), (Equation 3.14), and (Equation 3.20) which we state abstractly as

$$M\nu = b \tag{3.21}$$

where

$$M = \begin{pmatrix} \tilde{M}_{BC} & M_{BC} \\ \tilde{M}_{DN} & M_{DN} \end{pmatrix}, \quad \nu = \begin{pmatrix} \tilde{\mathbf{U}} \\ \tilde{\mathbf{W}} \\ \mathbf{U} \\ \mathbf{W} \end{pmatrix}, \quad \mathfrak{b} = \begin{pmatrix} \mathfrak{b}_{BC} \\ \mathfrak{b}_{DN} \end{pmatrix}. \tag{3.22}$$

In these

$$\tilde{M}_{BC} = \begin{pmatrix} 0 & 0 & 0 & 0 & 0 & 0 \\ 0 & 0 & 0 & 0 & 0 & 0 \\ \tilde{C}^{u,xx} & \tilde{C}^{u,xy} & \tilde{C}^{u,xz} & -\tilde{C}^{w,xx} & -\tilde{C}^{w,xy} & -\tilde{C}^{w,xz} \\ \tilde{C}^{u,yx} & \tilde{C}^{u,yy} & \tilde{C}^{u,yz} & -\tilde{C}^{w,yx} & -\tilde{C}^{w,yy} & -\tilde{C}^{w,yz} \\ \tilde{D}^{u,x} & \tilde{D}^{u,y} & \tilde{D}^{u,z} & 0 & 0 & 0 \\ 0 & 0 & 0 & \tilde{D}^{w,x} & \tilde{D}^{w,y} & \tilde{D}^{w,z} \end{pmatrix}, \tag{3.23a}$$

and

$$M_{BC} = \begin{pmatrix} S^{xx} & S^{xy} & S^{xz} & -S^{xx} & -S^{xy} & -S^{xz} \\ S^{yx} & S^{yy} & S^{yz} & -S^{yx} & -S^{yy} & -S^{yz} \\ C^{u,xx} & C^{u,xy} & C^{u,xz} & -C^{w,xx} & -C^{w,xy} & -C^{w,xz} \\ C^{u,yx} & C^{u,yy} & C^{u,yz} & -C^{w,yx} & -C^{w,yy} & -C^{w,yz} \\ D^{u,x} & D^{u,y} & D^{u,z} & 0 & 0 & 0 \\ 0 & 0 & 0 & D^{w,x} & D^{w,y} & D^{w,z} \end{pmatrix}, \tag{3.23b}$$

and

$$\tilde{M}_{DN} = \begin{pmatrix} A^{u} & 0 & 0 & 0 & 0 & 0 \\ 0 & A^{u} & 0 & 0 & 0 & 0 \\ 0 & 0 & A^{u} & 0 & 0 & 0 \\ 0 & 0 & 0 & A^{w} & 0 & 0 \\ 0 & 0 & 0 & 0 & A^{w} & 0 \\ 0 & 0 & 0 & 0 & 0 & A^{w} \end{pmatrix}, \tag{3.23c}$$

and

$$M_{DN} = \begin{pmatrix} -R^u & 0 & 0 & 0 & 0 & 0 \\ 0 & -R^u & 0 & 0 & 0 & 0 \\ 0 & 0 & -R^u & 0 & 0 & 0 \\ 0 & 0 & 0 & -R^w & 0 & 0 \\ 0 & 0 & 0 & 0 & -R^w & 0 \\ 0 & 0 & 0 & 0 & 0 & -R^w \end{pmatrix}, \tag{3.23d}$$

and

$$b_{BC} = \begin{pmatrix} -\zeta^y - (\partial_y g)\zeta^z \\ \zeta^x + (\partial_x g)\zeta^z \\ -\psi^y - (\partial_y g)\psi^z \\ \psi^x + (\partial_x g)\psi^z \\ 0 \\ 0 \end{pmatrix}, \quad b_{DN} = \begin{pmatrix} 0 \\ 0 \\ 0 \\ 0 \\ 0 \\ 0 \end{pmatrix}. \tag{3.23e}$$

3.8 A High–Order Perturbation of Surfaces (HOPS) Approach

Our High–Order Perturbation of Surfaces (HOPS) methodology for solving (Equation 3.21) is a straightforward application of regular perturbation theory. It can be shown that not only are the (known) linear operator $M = M(g) = M(\varepsilon f)$ and inhomogeneity $b = b(g) = b(\varepsilon f)$ *analytic* functions of ε for f sufficiently smooth (e.g., C^2, $C^{1+\alpha}$, or even Lipschitz), so is our unknown $\nu = \nu(g) = \nu(\varepsilon f)$ (53; 54; 24). Therefore we can make the strongly convergent expansions

$$\{M, \nu, b\} = \{M, \nu, b\}(g) = \{M, \nu, b\}(\varepsilon f) = \sum_{n=0}^{\infty} \{M_n, \nu_n, b_n\}(f)\varepsilon^n. \tag{3.24}$$

Insertion of these into (Equation 3.21) followed by equating at order ε^n yields

$$M_0 \nu_n = b_n - \sum_{\ell=0}^{n-1} M_{n-\ell}\nu_\ell. \tag{3.25}$$

Note that at each perturbation order, while one must *apply* the operators $M_{n-\ell}$, one need only *invert* the flat–interface operator M_0 (repeatedly). Once this has been accomplished for a range of orders $0 \leq n \leq N$ (delivering ν_n) one can form an approximate solution

$$\nu^N(x, y; \varepsilon) := \sum_{n=0}^{N} \nu_n(x, y)\varepsilon^n. \tag{3.26}$$

All that remains is to specify M_n and b_n. These come from (Equation 3.22) and it is clear that this will mandate expansions

$$\left\{\tilde{M}_{BC}, M_{BC}, \tilde{M}_{DN}, M_{DN}, b_{BC}, b_{DN}\right\}(\varepsilon f) = \sum_{n=0}^{\infty} \left\{\tilde{M}_{BC,n}, M_{BC,n}, \tilde{M}_{DN,n}, M_{DN,n}, b_{BC,n}, b_{DN,n}\right\}(f)\varepsilon^n.$$

This, in turn, requires forms for

$$\left\{S^{rs}, \tilde{C}^{m,rs}, C^{m,rs}, \tilde{D}^{m,r}, D^{m,r}, A^u, A^w, R^u, R^w, \zeta^r, \psi^r\right\} = \sum_{n=0}^{\infty} \left\{S_n^{rs}, \tilde{C}_n^{m,rs}, C_n^{m,rs}, \tilde{D}_n^{m,r}, D_n^{m,r}, A_n^u, A_n^w, R_n^u, R_n^w, \zeta_n^r, \psi_n^r\right\}(f)\varepsilon^n,$$

for $m \in \{u, w\}$ and $r, s \in \{x, y, z\}$. All of these are easily derived, and forms for $\{A_n^u, A_n^w, R_n^u, R_n^w, \zeta_n, \psi_n\}$ appear in (17). We presently specify the remainder.

From (Equation 3.8) we have the non–zero components

$$S_0^{xy} = -1, \quad S_1^{xz} = -(\partial_y f), \quad S_0^{yx} = 1, \quad S_1^{yz} = (\partial_x f).$$

(Equation 3.11), (Equation 3.12), and (Equation 3.13) give the non–zero members

$$\tilde{C}_0^{u,xy} = 1, \quad \tilde{C}_1^{u,xz} = (\partial_y f),$$

$$C_1^{u,xy} = -(\partial_x f)\partial_x - (\partial_y f)\partial_y, \quad C_0^{u,xz} = \partial_y, \quad C_2^{u,xz} = -(\partial_x f)(\partial_y f)\partial_x + (\partial_x f)^2\partial_y,$$

and

$$\tilde{C}_0^{u,yx} = -1, \quad \tilde{C}_1^{u,yz} = -(\partial_x f),$$

$$C_1^{u,yx} = (\partial_x f)\partial_x + (\partial_y f)\partial_y, \quad C_0^{u,yz} = -\partial_x, \quad C_2^{u,yz} = -(\partial_y f)^2\partial_x + (\partial_x f)(\partial_y f)\partial_y,$$

and

$$\tilde{C}_1^{u,zx} = -(\partial_y f), \quad \tilde{C}_1^{u,zy} = (\partial_x f),$$

$$C_0^{u,zx} = -\partial_y, \quad C_2^{u,zx} = (\partial_x f)(\partial_y f)\partial_x - (\partial_x f)^2\partial_y,$$

$$C_0^{u,zy} = \partial_x, \quad C_2^{u,zy} = (\partial_y f)^2\partial_x - (\partial_x f)(\partial_y f)\partial_y.$$

Similarly, (Equation 3.15), (Equation 3.16), and (Equation 3.17) deliver

$$\tilde{C}_0^{w,xy} = -1, \quad \tilde{C}_1^{w,xz} = -(\partial_y f),$$

$$C_1^{w,xy} = -(\partial_x f)\partial_x - (\partial_y f)\partial_y, \quad C_0^{w,xz} = \partial_y, \quad C_2^{w,xz} = -(\partial_x f)(\partial_y f)\partial_x + (\partial_x f)^2\partial_y,$$

and

$$\tilde{C}_0^{w,yx} = 1, \quad \tilde{C}_1^{w,yz} = (\partial_x f),$$

$$C_1^{w,yx} = (\partial_x f)\partial_x + (\partial_y f)\partial_y, \quad C_0^{w,yz} = -\partial_x, \quad C_2^{w,yz} = -(\partial_y f)^2\partial_x + (\partial_x f)(\partial_y f)\partial_y,$$

and

$$\tilde{C}_1^{w,zx} = (\partial_y f), \quad \tilde{C}_1^{w,zy} = -(\partial_x f),$$

$$C_0^{w,zx} = -\partial_y, \quad C_2^{w,zx} = (\partial_x f)(\partial_y f)\partial_x - (\partial_x f)^2\partial_y,$$

$$C_0^{w,zy} = \partial_x, \quad C_2^{w,zy} = (\partial_y f)^2\partial_x - (\partial_x f)(\partial_y f)\partial_y.$$

Finally, from (Equation 3.18) and (Equation 3.19) we find, respectively, the non–zero contributions

$$\tilde{D}_1^{u,x} = (\partial_x f), \quad \tilde{D}_1^{u,y} = (\partial_y f), \quad \tilde{D}_0^{u,z} = -1,$$

$$D_0^{u,x} = \partial_x, \quad D_2^{u,x} = (\partial_y f)^2 \partial_x - (\partial_x f)(\partial_y f)\partial_y,$$

$$D_0^{u,y} = \partial_y, \quad D_2^{u,y} = -(\partial_x f)(\partial_y f)\partial_x + (\partial_x f)^2 \partial_y,$$

$$D_1^{u,z} = (\partial_x f)\partial_x + (\partial_y f)\partial_y,$$

and

$$\tilde{D}_1^{w,x} = -(\partial_x f), \quad \tilde{D}_1^{w,y} = -(\partial_y f), \quad \tilde{D}_0^{w,z} = 1,$$

$$D_0^{w,x} = \partial_x, \quad D_2^{w,x} = (\partial_y f)^2 \partial_x - (\partial_x f)(\partial_y f)\partial_y,$$

$$D_0^{w,y} = \partial_y, \quad D_2^{w,y} = -(\partial_x f)(\partial_y f)\partial_x + (\partial_x f)^2 \partial_y,$$

$$D_1^{w,z} = (\partial_x f)\partial_x + (\partial_y f)\partial_y.$$

3.9 Numerical Results

We now point out that a numerical implementation of this algorithm is immediate. Indeed, we consider a HOPS approach to the solution of (Equation 3.21) which amounts to a numerical approximation of solutions to (Equation 3.25),

$$\nu_n = M_0^{-1} \left[b_n - \sum_{\ell=0}^{n-1} M_{n-\ell} \nu_\ell \right].$$

We approximate the members of the truncated Taylor series (Equation 3.26),

$$\nu_n(x,y) = \begin{pmatrix} \tilde{\mathbf{U}}_n(x,y) \\ \tilde{\mathbf{W}}_n(x,y) \\ \mathbf{U}_n(x,y) \\ \mathbf{W}_n(x,y) \end{pmatrix},$$

by

$$\nu_n^{N_x,N_y}(x,y) := \sum_{p=-N_x/2}^{N_x/2-1} \sum_{q=-N_y/2}^{N_y/2-1} \begin{pmatrix} \hat{\hat{U}}_{n,p,q}(x,y) \\ \hat{\hat{W}}_{n,p,q}(x,y) \\ \hat{U}_{n,p,q}(x,y) \\ \hat{W}_{n,p,q}(x,y) \end{pmatrix} e^{i\alpha_p x + i\beta_q y}.$$

The unknown coefficients are recovered upon demanding that (Equation 3.25) be true for these forms. Convolution products are computed using the FFT algorithm (55) and the only "discretization" is that we restrict to $-N_x/2 \le p \le N_x/2-1$ and $-N_y/2 \le q \le N_y/2-1$.

Of great importance is how the Taylor series in ε, (Equation 3.26), is to be summed. To be specific, to approximate ν we have just considered the truncation

$$\nu^{N_x,N_y,N}(x,y;\varepsilon) := \sum_{p=-N_x/2}^{N_x/2-1} \sum_{q=-N_y/2}^{N_y/2-1} \left(\sum_{n=0}^{N} \hat{\nu}_{p,q,n} \varepsilon^n \right) e^{i\alpha_p x + i\beta_q y},$$

which generates the Taylor polynomials

$$\hat{\nu}_{p,q}^N(\varepsilon) := \sum_{n=0}^{N} \hat{\nu}_{p,q,n} \varepsilon^n.$$

The Padé approximation (56) has been successfully used with HOPS methods on many occasions (see, e.g., (21; 54)), and we recommend its use here. Padé approximation simulate the truncated Taylor series $\hat{\nu}_{p,q}^N(\varepsilon)$ by

$$[L/M](\varepsilon) := \frac{a^L(\varepsilon)}{b^M(\varepsilon)} = \frac{\sum_{\ell=0}^{L} a_\ell \varepsilon^\ell}{1 + \sum_{m=1}^{M} b_m \varepsilon^m} \tag{3.27}$$

where $L + M = N$ and

$$[L/M](\varepsilon) = \hat{\nu}_{p,q}^N(\varepsilon) + \mathcal{O}(\varepsilon^{L+M+1});$$

well–known formulas for the coefficients $\{a_\ell, b_m\}$ can be found in (56). This approximant has remarkable properties of enhanced convergence, which can be found in § 2.2 of Baker & Graves–Morris (56) and § 8.3 of Bender & Orszag (57).

3.10 Validation

For the problem of plane–wave scattering by a (non–flat) diffraction grating there are, of course, no exact solutions. Therefore, in order to validate our code, we compare results of our simulations with those generated from Field Expansions (FE) simulations described and previously verified in (27). Among the myriad choices of quantities to measure we have selected the zeroth ("specular") reflected efficiency, $e^u_{0,0}$, as it is the precipitous drop in this quantity which signals the onset of a Surface Plasmon Resonance (50; 51; 52).

With this in mind we chose a particular physical configuration which is motivated by the seminal work of Bruno & Reitich (22) on the FE scheme for simulating the vector Maxwell equations for a doubly layered medium. We consider the sinusoidal biperiodic grating shape specified by

$$f(x,y) = \frac{1}{4}\left[\cos\left(\frac{2\pi x}{d}\right) + \cos\left(\frac{2\pi y}{d}\right)\right], \tag{3.28a}$$

so that $d_1 = d_2 = d$. We chose their wavelength–to–period ratio $\lambda/d = 0.83$, but did not restrict to normally incident radiation. Indeed, if we express

$$\alpha = (2\pi/\lambda)\nu^u \sin(\theta)\cos(\phi), \quad \beta = (2\pi/\lambda)\nu^u \sin(\theta)\sin(\phi), \tag{3.28b}$$

$$k^u = (2\pi/\lambda)\nu^u, \quad k^w = (2\pi/\lambda)\nu^w, \tag{3.28c}$$

$$\gamma^u = \sqrt{(k^u)^2 - \alpha^2 - \beta^2}, \quad \gamma^w = \sqrt{(k^w)^2 - \alpha^2 - \beta^2}, \tag{3.28d}$$

where ν^m is the index of refraction of layer m, then we chose

$$\theta = 10(2\pi/360), \quad \phi = 5(2\pi/360), \quad \nu^u = 1, \quad \nu^w = 2. \tag{3.28e}$$

To conclude the specification of the configuration, we selected

$$\varepsilon/d = 0.003, 0.01, 0.03, 0.1, \quad d = 0.500. \tag{3.28f}$$

For numerical parameters we chose

$$N_x = N_y = 16, \quad N = 10,$$

and computed the relative error between our new approach (denoted "FIE") and the FE algorithm:

$$\text{Error} = \frac{\left|e_{0,0}^{u,\text{FIE}} - e_{0,0}^{u,\text{FE}}\right|}{\left|e_{0,0}^{u,\text{FE}}\right|}.$$

In Figure 3.2 we study the convergence of our new methodology for various perturbation orders N utilizing Padé approximation as the profile height ε is varied.

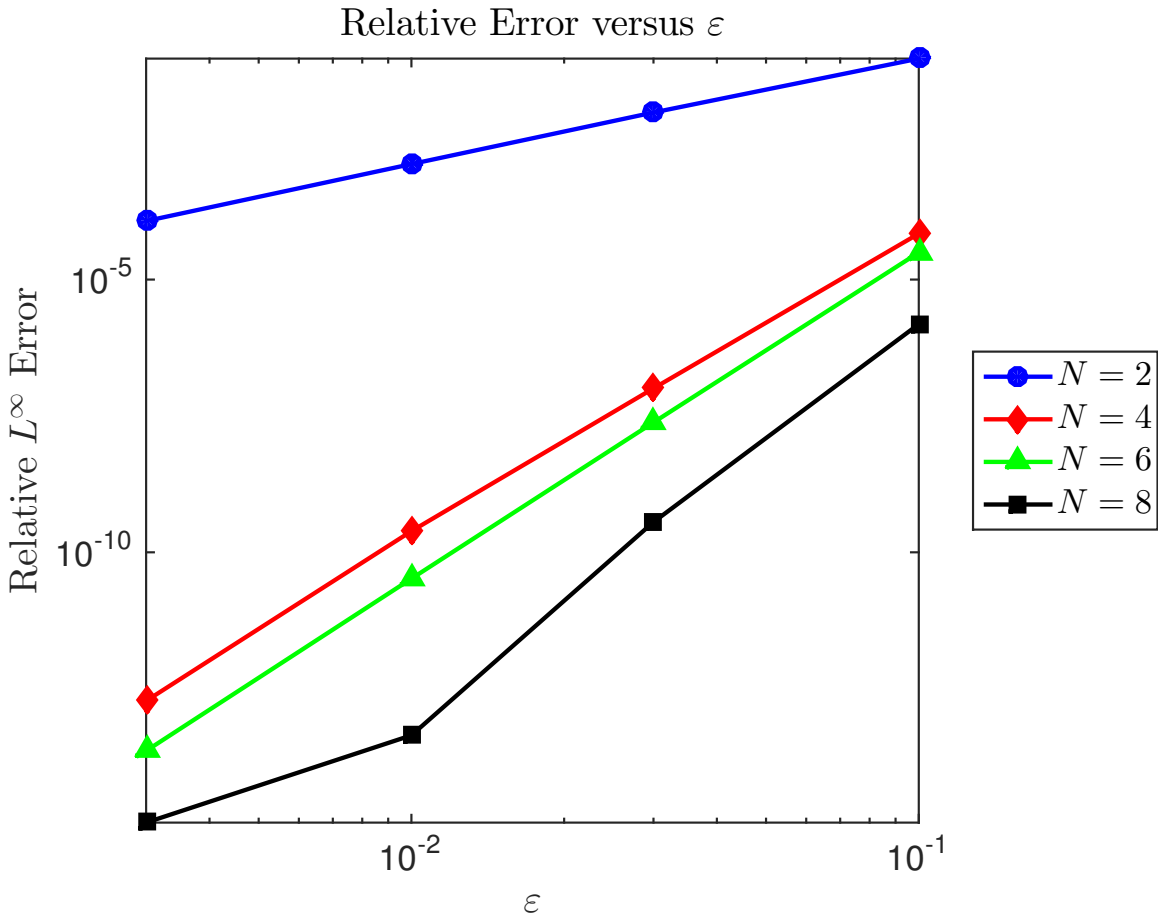

Figure 14. Relative error for 3-D two layer Maxwell problem

Figure 3.2: Relative error versus perturbation parameter ε for various perturbation orders N (with $[N/2, N/2]$ Padé approximation). Results for the (Equation 3.28), with $N_x = N_y = 16$.

In Figure 3.3 we display results of our convergence study for different values of the height ε as N is refined.

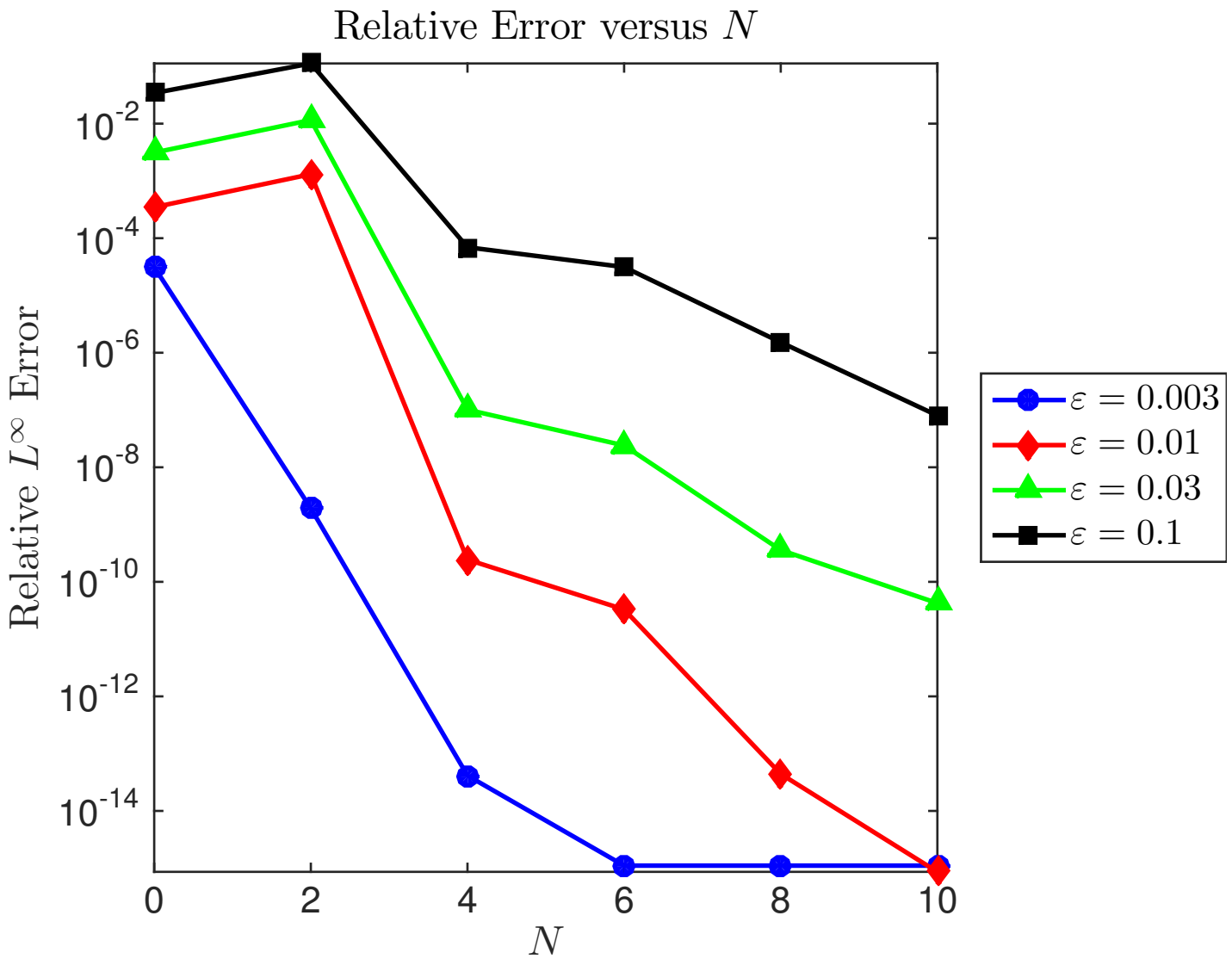

Figure 3.3: Relative error versus perturbation order N (with [N/2, N/2] Padé approximation) for various perturbation parameters ε. Results for the (Equation 3.28), with $N_x = N_y = 16$.

In each of these figures we note the rapid and robust convergence of our new approach to the results of the validated, high–order accurate FE methodology (27).

3.11 Simulation of Reflectivity Maps

To conclude, we considered configurations inspired by the simulations of the laboratory of S.–H. Oh (Minnesota), particularly the Surface Plasmon Resonance (SPR) sensing devices studied in (46; 49). In these a two–dimensional sensor was studied featuring a corrugated

insulator/conductor interface. While we are unable at present to study the third insulator layer featured there, we are able to add three–dimensional effects and, with very little trouble, change the types of the insulator and/or conductor.

We retained the grating interface shape f defined in (Equation 3.28a), chose vacuum as the insulator above the interface so that $\nu^u = 1$, and filled the lower layer with either gold or silver. The indices of refraction of these metals are the subject of current research, and for these we selected Lorentz models

$$\varepsilon^\sigma = \varepsilon_\infty^\sigma + \sum_{j=1}^{6} \frac{\Delta_j^\sigma}{-a_j^\sigma \omega^2 - ib_j^\sigma \omega + c_j^\sigma}, \quad \sigma \in \{\mathrm{Au}, \mathrm{Ag}\},$$

where $\omega = 2\pi/\lambda$, and the parameters $\varepsilon_\infty^\sigma$, Δ_j^σ, a_j^σ, b_j^σ, c_j^σ can be found in (58). For physical and numerical parameters we chose

$$\theta = 0, \quad \phi = 0,$$

$$h = \varepsilon = 0, \ldots, 0.200, \quad d_1 = d_2 = 0.650,$$

$$N_x = N_y = 12, \quad N = 0, \ldots, 8.$$

In Figure 3.4 we display the Reflectivity Map, $R(\lambda, h)$, (Equation 3.5), for this configuration which shows a strong resonance around $\lambda = 670$ nm and $h = 90$ nm.

Figure 3.4: Reflectivity Map for the two–layer vacuum/gold configuration, $R(\lambda, h)$, versus incident wavelength, λ, and deformation height $h = \varepsilon$. Results for the sinusoidal shape (Equation 3.28a) with $N_x = N_y = 12$, [4/4] Padé approximant.

By contrast, in Figure 3.5 we display R, (Equation 3.5), where we have replaced gold with silver. This shows a much more sensitive (narrower in λ) resonance at the new values

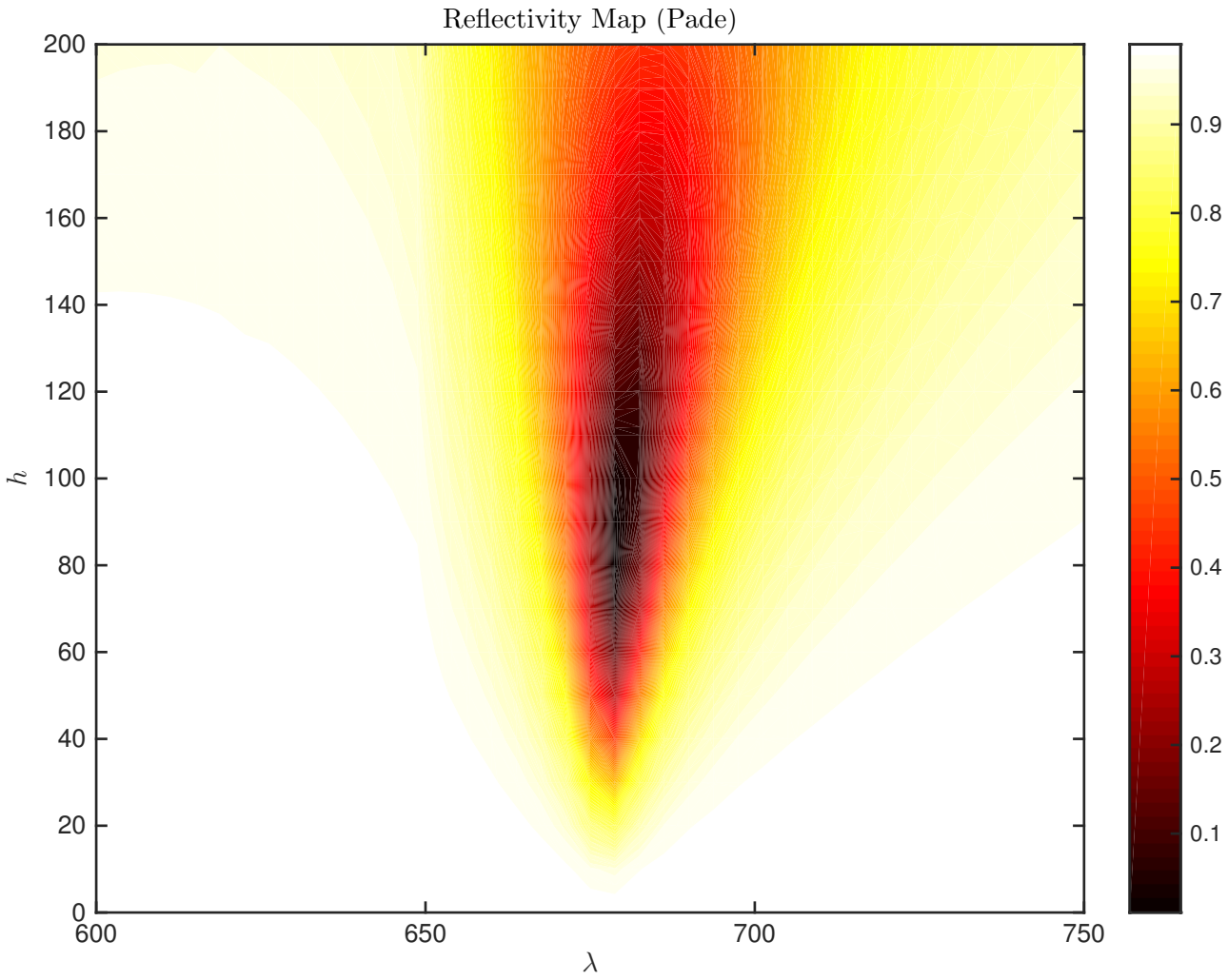

Figure 15. Reflectivity Map for two-layer vaccum/gold configuration for Maxwell problem

$\lambda = 665$ nm and $h = 60$ nm.

Figure 3.5: Reflectivity Map for the two–layer vacuum/silver configuration, $R(\lambda, h)$, versus incident wavelength, λ, and deformation height $h = \varepsilon$. Results for the sinusoidal shape (Equation 3.28a) with $N_x = N_y = 12$, [4/4] Padé approximant.

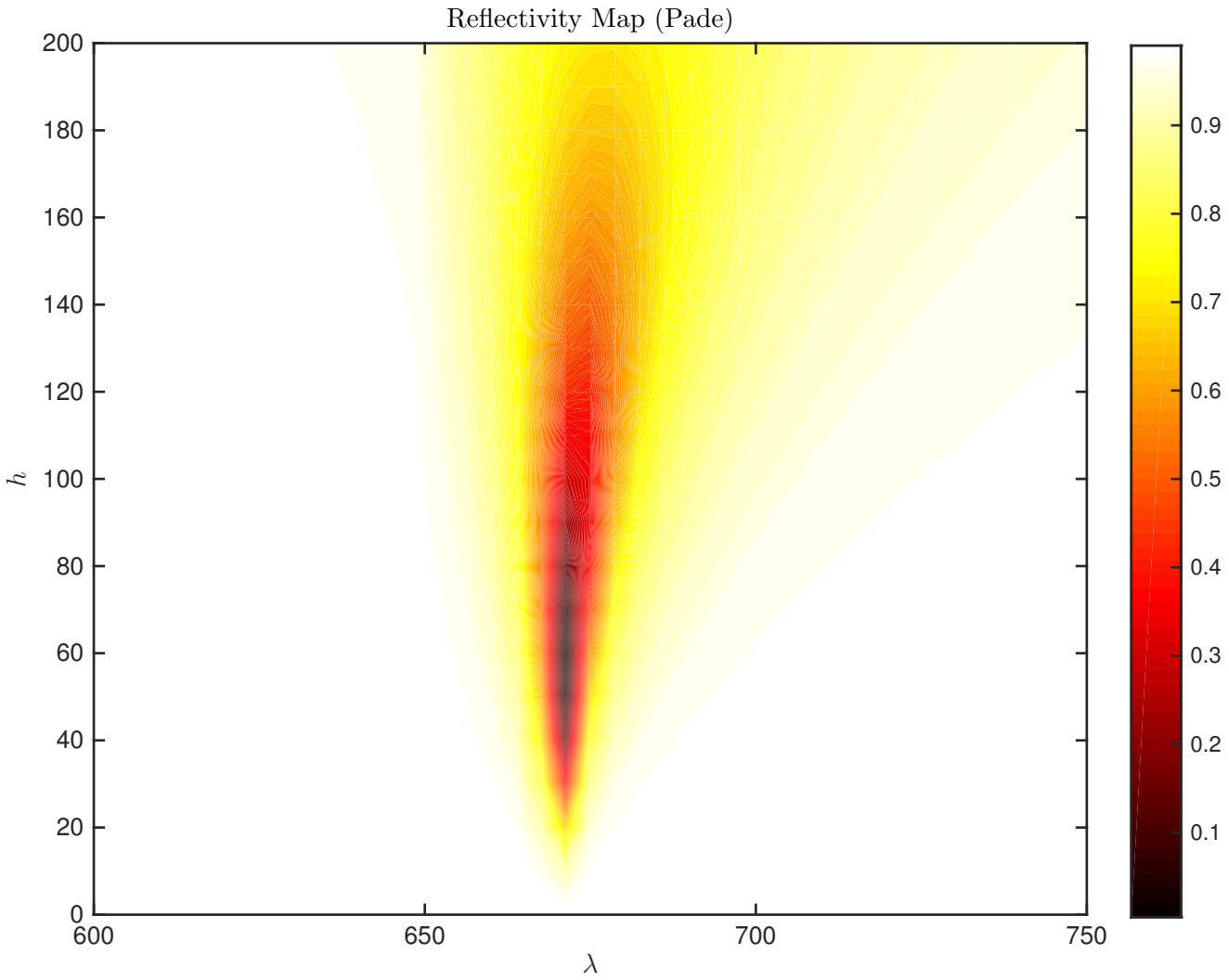

Figure 16. Reflectivity Map for two-layer vaccum/silver configuration for Maxwell problem

CHAPTER 4

CONCLUSION

We first implemented the HOPS algorithm designed by Nicholls for "Two Dimensional Helmholtz equation" by inverting the flat interface operator for every wavenumber there by reducing the size of the linear system involved. This new approach resulted in a linear system with better condition number and lower dimensions. Using this approach, we successfully reproduced the Resonance phenomenon achieved by Bruno and Reitich for two layers and by Nicholls and Maxwell for multiple layer(21 layers). The performance improvement is significant for the 21-layers case. Encouraged by our results, we successfully built on the framework developed for the scalar Helmholtz equation to solve the 3D vector Maxwell equations for single interface separating two layers. Our results confirmed our assertions about the benefits of this method compared to others.

CHAPTER 5

FUTURE DIRECTION

Going forward, we want to reduce the number of unknowns for three dimensional scattering in the two layer case by writing the lower layer Dirichlet and Neumann trace parameters in terms of the upper layer Dirichlet and Neumann trace parameters as done in the case of two dimensional scattering. This would reduce the size of our linear system by a factor 6. We later wish to extend our three dimensional scattering algorithm to handle multiple layers (greater than 2).

CITED LITERATURE

1. Schadle, A., Zschiedrich, L., Burger, S., Klose, R., and Schmidt, F.: Domain decomposition method for Maxwell's equations: Scattering off periodic structures. Journal of Computational Physics, 226(1):477–493, 2007.

2. Demesy, G., Zolla, F., Nicolet, A., and Commandre, M.: Versatile full–vectorial finite element model for crossed gratings. Optics Letters, 34(14):2216–2219, 2009.

3. Huber, M., Schoberl, J., Sinwel, A., and Zaglmayr, S.: Simulation of diffraction in periodic media with a coupled finite element and plane wave approach. SIAM Journal on Scientific Computation, 31(2):1500–1517, 2009.

4. Stannigel, K., Konig, M., Niegemann, J., and Busch, K.: Discontinuous Galerkin time-domain computations of metallic nanostructures. Optics Express, 17:14934–14947, 2009.

5. Christensen, D. and Fowers, D.: Modeling SPR sensors with the finite-difference time-domain method. Biosensors and Bioelectronics, 11:677–684, 1996.

6. Sai, H., Kanamori, Y., Hane, K., and Yugami, H.: Numerical study on spectral properties of Tungsten one-dimensional surface-relief gratings for spectrally selective devices. J. Opt. Soc. Am. A, 22:1805–1813, 2005.

7. Lindquist, N., Johnson, T., Norris, D., and Oh, S.-H.: Monolithic integration of continuously tunable plasmonic nanostructures. Nano Lett., 11:3526–3530, 2011.

8. Berenger, J.-P.: A perfectly matched layer for the absorption of electromagnetic waves. J. Comput. Phys., 114(2):185–200, 1994.

9. Givoli, D.: Nonreflecting boundary conditions. J. Comput. Phys., 94(1):1–29, 1991.

10. Givoli, D.: Numerical methods for problems in infinite domains, volume 33 of Studies in Applied Mechanics. Amsterdam, Elsevier Scientific Publishing Co., 1992.

11. Givoli, D.: Recent advances in the DtN FE method. Arch. Comput. Methods Engrg., 6(2):71–116, 1999.

12. Colton, D. and Kress, R.: Inverse acoustic and electromagnetic scattering theory. Berlin, Springer-Verlag, second edition, 1998.

13. Greengard, L. and Rokhlin, V.: A fast algorithm for particle simulations. J. Comput. Phys., 73(2):325–348, 1987.

14. Reitich, F. and Tamma, K.: State–of–the–art, trends, and directions in computational electromagnetics. CMES Comput. Model. Eng. Sci., 5(4):287–294, 2004.

15. Kurkcu, H. and Reitich, F.: Stable and efficient evaluation of periodized Green's functions for the Helmholtz equation at high frequencies. J. Comput. Phys., 228(1):75–95, 2009.

16. Ambrose, D. and Nicholls, D. P.: Fokas integral equations for three dimensional layered–media scattering. Journal of Computational Physics, 276:1–25, 2014.

17. Nicholls, D. P.: A high–order perturbation of surfaces (HOPS) approach to Fokas integral equations: Three–dimensional layered media scattering. Quarterly of Applied Mathematics (to appear), 2014.

18. Rayleigh, L.: On the dynamical theory of gratings. Proc. Roy. Soc. London, A79:399–416, 1907.

19. Rice, S. O.: Reflection of electromagnetic waves from slightly rough surfaces. Comm. Pure Appl. Math., 4:351–378, 1951.

20. Bruno, O. P. and Reitich, F.: Numerical solution of diffraction problems: A method of variation of boundaries. J. Opt. Soc. Am. A, 10(6):1168–1175, 1993.

21. Bruno, O. P. and Reitich, F.: Numerical solution of diffraction problems: A method of variation of boundaries. II. Finitely conducting gratings, Padé approximants, and singularities. J. Opt. Soc. Am. A, 10(11):2307–2316, 1993.

22. Bruno, O. P. and Reitich, F.: Numerical solution of diffraction problems: A method of variation of boundaries. III. Doubly periodic gratings. J. Opt. Soc. Am. A, 10(12):2551–2562, 1993.

23. Nicholls, D. P. and Reitich, F.: Shape deformations in rough surface scattering: Cancellations, conditioning, and convergence. J. Opt. Soc. Am. A, 21(4):590–605, 2004.

24. Nicholls, D. P. and Reitich, F.: Shape deformations in rough surface scattering: Improved algorithms. J. Opt. Soc. Am. A, 21(4):606–621, 2004.

25. Nicholls, D. P. and Reitich, F.: Boundary perturbation methods for high–frequency acoustic scattering: Shallow periodic gratings. J. Acoust. Soc. Amer., 123(5):2531–2541, 2008.

26. Malcolm, A. and Nicholls, D. P.: A field expansions method for scattering by periodic multilayered media. Journal of the Acoustical Society of America, 129(4):1783–1793, 2011.

27. Nicholls, D. P.: A method of field expansions for vector electromagnetic scattering by layered periodic crossed gratings. Journal of the Optical Society of America, A (to appear), 2015.

28. Milder, D. M.: An improved formalism for rough-surface scattering of acoustic and electromagnetic waves. In Proceedings of SPIE - The International Society for Optical Engineering (San Diego, 1991), volume 1558, pages 213–221. Bellingham, WA, Int. Soc. for Optical Engineering, 1991.

29. Milder, D. M.: An improved formalism for wave scattering from rough surfaces. J. Acoust. Soc. Am., 89(2):529–541, 1991.

30. Milder, D. M. and Sharp, H. T.: Efficient computation of rough surface scattering. In Mathematical and numerical aspects of wave propagation phenomena (Strasbourg, 1991), pages 314–322. Philadelphia, PA, SIAM, 1991.

31. Milder, D. M. and Sharp, H. T.: An improved formalism for rough surface scattering. ii: Numerical trials in three dimensions. J. Acoust. Soc. Am., 91(5):2620–2626, 1992.

32. Milder, D. M.: Role of the admittance operator in rough-surface scattering. J. Acoust. Soc. Am., 100(2):759–768, 1996.

33. Milder, D. M.: An improved formalism for electromagnetic scattering from a perfectly conducting rough surface. Radio Science, 31(6):1369–1376, 1996.

34. Coifman, R., Goldberg, M., Hrycak, T., Israeli, M., and Rokhlin, V.: An improved operator expansion algorithm for direct and inverse scattering computations. Waves Random Media, 9(3):441–457, 1999.

35. Fokas, A. S.: A unified approach to boundary value problems, volume 78 of CBMS-NSF Regional Conference Series in Applied Mathematics. Philadelphia, PA, Society for Industrial and Applied Mathematics (SIAM), 2008.

36. Ablowitz, M. J., Fokas, A. S., and Musslimani, Z. H.: On a new non-local formulation of water waves. J. Fluid Mech., 562:313–343, 2006.

37. Spence, E. A. and Fokas, A. S.: A new transform method I: domain-dependent fundamental solutions and integral representations. Proc. R. Soc. Lond. Ser. A Math. Phys. Eng. Sci., 466(2120):2259–2281, 2010.

38. Spence, E. A. and Fokas, A. S.: A new transform method II: the global relation and boundary-value problems in polar coordinates. Proc. R. Soc. Lond. Ser. A Math. Phys. Eng. Sci., 466(2120):2283–2307, 2010.

39. Petit, R.: Electromagnetic theory of gratings. Berlin, Springer-Verlag, 1980.

40. Bruno, P. and Reitich, F.: Solution of a boundary value problem for helmholtz equation via variation of the boundary into the complex domain. Proc. R. Soc. Edinburgh Sect. A, 122:317–340, 1992.

41. Nicholls, D. P.: Three-dimensional acoustic scattering by layered media: A novel surface formulation with operator expansions implementation. 468:731–758, 2012.

42. Nicholls, D. P. and Reitich, F.: Stability of high-order perturbative methods for the computation of Dirichlet-Neumann operators. J. Comput. Phys., 170(1):276–298, 2001.

43. Jackson, J. D.: Classical electrodynamics. New York, John Wiley and Sons Inc., second edition, 1975.

44. Homola, J.: Surface plasmon resonance sensors for detection of chemical and biological species. Chemical Reviews, 108(2):462–493, 2008.

45. Im, H., Lee, S. H., Wittenberg, N. J., Johnson, T. W., Lindquist, N. C., Nagpal, P., Norris, D. J., and Oh, S. H.: Template-stripped smooth Ag nanohole arrays with silica shells for surface plasmon resonance biosensing. ACS Nano, 5:6244–6253, 2011.

46. Lindquist, N. C., Johnson, T. W., Jose, J., Otto, L. M., and Oh, S.-H.: Ultrasmooth metallic films with buried nanostructures for backside reflection-mode plasmonic biosensing. Annalen der Physik, 524:687–696, 2012.

47. Jose, J., Jordan, L., Johnson, T., Lee, S., Wittenberg, N., and Oh, S.: Topographically flat substrates with embedded nanoplasmonic devices for biosensing. Adv Funct Mater, 23:2812–2820, 2013.

48. Reitich, F., Johnson, T., Oh, S.-H., and Meyer, G.: A fast and high-order accurate boundary perturbation method for characterization and design in nanoplasmonics. Journal of the Optical Society of America, A, 30:2175–2187, 2013.

49. Nicholls, D. P., Reitich, F., Johnson, T., and Oh, S.-H.: Fast high–order perturbation of surfaces (HOPS) methods for simulation of multi–layer plasmonic devices and metamaterials. Journal of the Optical Society of America, A, 31(8):1820–1831, 2014.

50. Raether, H.: Surface plasmons on smooth and rough surfaces and on gratings. Berlin, Springer, 1988.

51. Maier, S.: Plasmonics: Fundamentals and Applications. New York, Springer, 2007.

52. Enoch, S. and Bonod, N.: Plasmonics: From Basics to Advanced Topics. Springer Series in Optical Sciences. New York, Springer, 2012.

53. Nicholls, D. P. and Reitich, F.: A new approach to analyticity of Dirichlet-Neumann operators. Proc. Roy. Soc. Edinburgh Sect. A, 131(6):1411–1433, 2001.

54. Nicholls, D. P. and Reitich, F.: Analytic continuation of Dirichlet-Neumann operators. Numer. Math., 94(1):107–146, 2003.

55. Gottlieb, D. and Orszag, S. A.: Numerical analysis of spectral methods: theory and applications. Philadelphia, Pa., Society for Industrial and Applied Mathematics, 1977. CBMS-NSF Regional Conference Series in Applied Mathematics, No. 26.

56. Baker, Jr., G. A. and Graves-Morris, P.: Padé approximants. Cambridge, Cambridge University Press, second edition, 1996.

57. Bender, C. M. and Orszag, S. A.: Advanced mathematical methods for scientists and engineers. New York, McGraw-Hill Book Co., 1978. International Series in Pure and Applied Mathematics.

58. Rakic, A., Djurisic, A., Elazar, J., and Majewski, M.: Optical properties of metallic films for vertical-cavity optoelectronic devices. Applied Optics, 37(22):5271–5283, 1998.

VENU MADHAV TAMMALI
323 W. Concord Pl, Chicago, IL 60614 | Phone : (612)545-8028 | Email : vmt221@nyu.edu

EDUCATION

UNIVERSITY OF ILLINOIS AT CHICAGO — Chicago, IL.
PhD – Applied/Computational Mathematics (May 2015) — **G.P.A:- 4.0/ 4.0.**

COURANT INSTITUTE, NEW YORK UNIVERSITY — New York, NY.
MS – Applied Mathematics (Sep 2012) — **G.P.A:- 3.8/ 4.0**.

VASAVI COLLEGE OF ENGINEERING, OSMANIA UNIVERSITY — Hyderabad, INDIA.
BE - Electronics /Computer Science Engineering(May 2004) — **(77/100).**

SKILLS

C/C++, JAVA, STRUTS, J2EE, SQL, PLSQL, ETL, MATLAB, **R,** Regression Analysis, PCA Analysis, Data Compression, Data mining.

SELECTED COURSEWORK

Computational Finance, Pricing options, Numerical methods in PDE, Stochastic Calculus, Derivative Securities, Computer Algorithms, Object-Oriented Programming, Data mining, Machine Learning.

CERTIFICATIONS

Oracle Certified Database Professional.

RESEARCH EXPERIENCE

05/13 – Present — **Compression of large multidimensional data (Tensors), Compressive Sensing, Data Compression using Random Projections**
Advisor: - Prof. Shmuel Friedland.

- Formulated and coded fast algorithms in **C++** to compress large sized multi dimensional data(Tensors) by low rank approximation.
- One of our proposed algorithm is the fastest among the available.

01/14 – Present — **Solve Maxwell equations using Boundary Perturbation Methods.**
Advisor: - Prof. David Nicholls.

- Formulated and coded fast algorithms in **C++** to solve Maxwell equations satisfied by Electro-Magnetic field scattered by multi layered 3D-surfaces.

02/11 - 05/11 — **Back test Statistical Arbitrage in the US Equities Market**
Advisor: - Prof Marco Avellaneda.

- Successfully tested Professor's strategy on S&P500 and NYSE historical data. The implementation was done in **C++.**

INDUSTRY EXPERIENCE

05/2014 - 09/2014 — **Research Scientist Intern Argonne National Lab Chicago, Illinois.**
Implemented Spectral element methods in **C++** to solve Convection-diffusion equation in 3D domain.

05/2012 – 09/2012 — **Financial Programmer Nationwide Financial Columbus, Ohio.**
Optimized **JAVA** code that handle trades between Nationwide and N.S.C.C (National Securities Clearing Corporation).

04/2008 – 9/2010 — **Software Design Engineer Blue Cross Blue Shield Jacksonville, Florida**.
Designed and developed the Billing and Invoice architecture for various Medicare and Med advantage products of BCBSFL. The architecture has been selected by BCBS as the base for implementing health care reform changes.

10/2004 – 11/2007 — **Software Engineer Infosys Hyderabad, India**
Customized Finacle product (Infosys Core banking product) as per Specifications of the bank.

ACHIEVEMENTS

Achieved Rank **756/120k** in state level engineering test (**EAMCET**).
Achieved **97** percentile in Graduate Aptitude test for Engineers (**GATE**).
Achieved **99** percentile in **GMAT (760/800)**.